Master Thesis

Spatial Control of the Threshold Voltages of Organic Transistors by Stamping

（スタンプ法による有機トランジスタの閾値電圧の局所制御）

Adviser　Professor Takao Someya

Submitted Feb. 2012

Department of Electrical Engineering
and Information Systems
Graduate School of Engineering
The University of Tokyo

37-106491 Ikue Hirata

Contents

Chapter 1

Introduction

1.1 Background

Since the invention in 1940's by Bardeen and Brattain [1], transistors have occupied an essential role in electronic devices. Based on transistors, transistors with MOS (metal-oxide semiconductor) structure and semiconductor lasers, and photovoltaic cells are developed. Today, those devices are essential components in electronic deices from home electrical appliances such as televisions and refrigerators to highly-computerized society. In addition, smart grid, a model of energy-saving society, practical realization of which has been accelerated after the Great East Japan Earthquake in March, 2011, largely depends on those devices.

One of the transistor technologies that improved the performances of data servers, information instrument, and even rice cookers is integration. By the advance of semiconductor fabrication and material technologies, the size of a transistor is decreased by the Moore's law. By the scaling-down, the performances of highly-integrated circuits, or VLSI (very-large-scale integration), were dramatically increased.

However, transistor fabrication faces the limitation of the integration. The high integration made the quantum effect non-negligible and the benefits of scaling become ineffective. Also, new technology always needs new facilities and the equipment investment may not be recouped. Now, the improvement of the performance is researched by the means of new structures, such as Fin-FET [2], and new materials with high electron mobility, such as Ge and compound semiconductors.

Recently, beside transistors based on inorganic materials as described above, transistors based on organic materials have attracted much attention because of their properties to realize a new class of devices.

One of the typical properties of organic devices is flexibility. The fabrication process of organic transistors is done under low temperature, the maximum of 100°C , while the fabrication process of inorganic transistors needs the maximum temperature of 1200°C to form SiO_2 on Si substrate. This low temperature enables the fabrication on flexible plastic substrate such as polyimide and Polyethylene naphthalate (PEN). Thanks to the

flexibility of the substrate and the organic material itself, the devices become mechanically flexible. Other specific property of organic devices is fabrication process, known as solution process, in which material depositions are done with solution. Besides the conventional vacuum evaporation method, many forms of solution process, such as dipping, spin-coating, and printing, are widely used in fabrication of organic electronics. In combination with large-scale printing method, process advantages enable industrial mass-production process, typically known as roll-to-roll, which decreases fabrication time, steps, and cost drastically.

Though the operation frequency of organic transistors is quite lower than inorganic transistors, due to the low mobility of 1–10 $cm^2/V{\cdot}s$, by making the most of the characteristics of organic devices, fabrication by solution process and flexibility, the new phase of electronics becomes possible. Thanks to the advance in fabrication process and materials, the electric properties of organic transistors reached up to amorphous silicon transistors [3], large-scale and complex organic circuits such as flexible displays [4, 5], radio frequency identification (RFID) tags [6], processors[7], and shift registers[8] are already demonstrated.

In Someya and Sekitani Laboratory, large-scale or flexible organic devices such as artificial electronic skin [9, 10], sheet scanner [11], braille sheet [12], large-area sensor arrays [13, 14], and stretchable display [15] are fabricated.

As in inorganic transistor fabrication, device parameter countability is essential in the fabrication of highly complex circuits for the reliable operation. Especially, large static noise margin (SNM) is indispensable for the successful suppression of inadvertent switching events in the unavoidable presence of electronic noise in practical use [16]. For large SNM, precise and deterministic control of the threshold voltage of transistors is required. However, because of the intrinsic properties of organic materials, such as instability of molecules, uncontrollably of trap density in crystal, process steps, and smaller mobility, it is a challenge to control the device properties, especially to control each transistor on a substrate.

By establishing a robust and simple method to control device characteristics, the possibility of organic electronics is expanded and highly complex circuits in large-scale and on flexible substrates to fully exploit the advantages of organic electronics is realized.

1.2 Motivation and Purpose of This Research

The purpose in this study is to demonstrate the possibility and to establish the process of spatial control of transistors by one of the soft-lithography methods, stamping. In this study, the method to control the threshold voltage is focused on using self-assembled monolayers (SAMs). Other methods and discussion on comparison of the methods are described in Section 2.4.

So far, the threshold voltage shift by using fluoro-terminated SAM is observed [17] and control is demonstrated [18]. The problem of using SAM is that this process is whole-

substrate process, which means that all transistors on a substrate have uniform threshold voltage. To overcome this problem and to form more than two species of SAMs on a substrate in different region simultaneously, stamping method is applied. The spatial formation of SAMs is demonstrated by Zschieschang et al. [19]

In this study, the control of threshold voltage using SAMs and the partial formation was combined to demonstrate spatial control of the threshold voltages. To ensure the equivalence of the stamping and conventional dipping, electrical properties and uniformness of the SAMs and transistors by stamping were compared with SAMs and transistors by dipping. Also, the robustness of the formation process was proved and the process steps were optimized to increase productivity. Furthermore, the structure of stamped SAMs was closely investigated, which was not revealed before. The stamped SAMs were then applied to load-inverter circuit to control the turn-on voltage.

1.3 Overview of Thesis

The overall structure of this study takes the form of seven chapters, including this introductory chapter. Chapter two explains the principles and electric property control of organic transistors. Related studies on the threshold voltage control is introduced and discussed. The third chapter is focused on the fabrication of organic transistors and circuits. The stamping process, which is the main topic, is explained in detail. The fourth chapter presents the characterization methods of transistors and thin films of organic compounds. Chapter five explains the experimental procedure, results, and discussion of stamping process optimization. Chapter six presents the experimental procedure, results, and discussion of threshold voltage control and application of the method to circuit using two different species of SAMs. Finally, the conclusion gives a brief summary and areas for further research.

Chapter 2

Organic Transistors

2.1 Operation Principles [20]

2.1.1 Structure

A general structure of an organic transistor is shown in Fig. 2.1(a). Transistors with organic semiconductors are often fabricated in the structure of thin film transistor (TFT). A TFT is a metal/insulator/semiconductor (MIS) structured field-effect transistor (MISFET). The device structure and the operation principle is similar to those of metal/oxide/silicon field-effect transistors (MOSFETs) and silicon on insulator (SOI). There are two types for

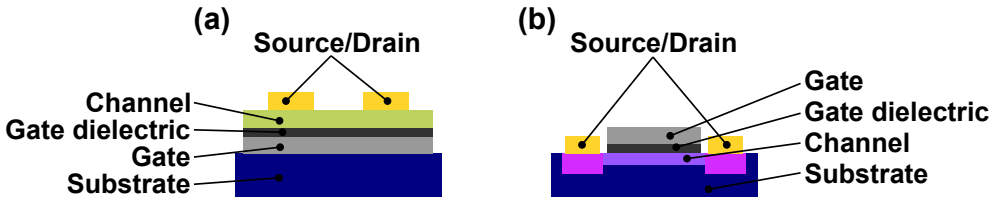

Figure 2.1: Cross-section view of transistor structure. (a) A TFT with bottom-gate and top-contact. (b) A MOSFET.

the structure of TFTs, top-gate top-contact, bottom-gate top-contact, top-gate bottom-contact, and bottom-gate bottom-contact. The types are differentiated by the geometries of gate electrode and source/drain electrodes. Typical inorganic MOSFETs are classified as top-gate top-contact. In the fabrication process of top-contact geometry, source/drain electrodes are formed after the semiconductor layer is formed on gate dielectric, while in the fabrication process of bottom-contact geometry source/drain electrodes are formed before the formation of organic semiconductor layer. The advantages of the top-contact geometry is that the formation of semiconductor layer on uniform material is enabled therefore the uniformity of the semiconductor is better than in bottom-contact geometry and carrier injection barrier height is decreased. In general, transistors with top-contact geometry are expected to have larger mobility than transistors with bottom-gate geometry. However, the fabrication method of the source/drain electrodes is limited because

the semiconductor layer is damaged by methods such as lithography and solution process.

In this work, top-contact bottom-gate geometry is adopted.

2.1.2 Field Effect

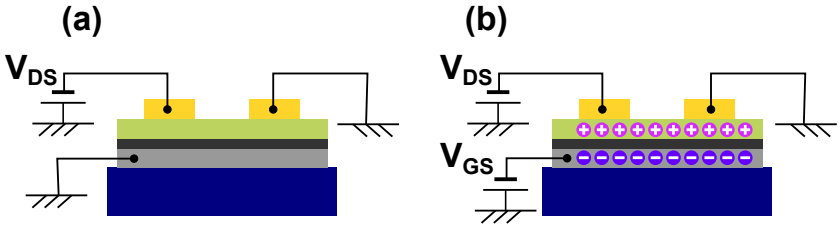

Figure 2.2: Schematics of the operation principles of TFTs. (a) Off state. (b) On state.

Schematic images of the operation principle of is shown in Fig. 2.2. Suppose gate voltage V_{GS} is applied, difference in potential of the drain electrode and the source electrode V_{DS} is 0, and the source electrode is grounded. The gate electrode and the channel region form a parallel plate type capacitor, therefore charges are induced at the interface of the channel region and the insulator. The amount of total charge at the channel is explained as

$$q_{\mathrm{a}} = -c_{\mathrm{i}} V_{\mathrm{GS}} \tag{2.1a}$$

$$c_{\mathrm{i}} = \frac{\epsilon_{\mathrm{i}}}{d} \tag{2.1b}$$

where q_{a} is the charge density per unit area in the channel region, c_{i} is the capacitance of the gate insulator per unit area, ϵ_{i} is the permittance of the gate insulator, d is the thickness of the gate insulator, $V_{\mathrm{GS}} = V_{\mathrm{G}} - V_{\mathrm{S}}$ is the gate–source voltage. Note that in p-type transistor, the source electrode is grounded and negative bias voltage is applied to the gate electrode, *i.e.*$V_{\mathrm{GS}} < 0$. Therefore, the induced charge q_{a} in the channel region is positive.

The charge density consists of two parts, free charge (carrier) q_{c} and trap state in the semiconductor layer q_{t}. q_{c} is explained as

$$q_{\mathrm{c}} = q_{\mathrm{a}} - q_{\mathrm{t}} = (-c_{\mathrm{i}} V_{\mathrm{GS}}) - q N_{\mathrm{t}} = -c_{\mathrm{i}}(V_{\mathrm{GS}} - V_{\mathrm{th}}) \tag{2.2a}$$

$$N_t = \frac{q_{\mathrm{t}}}{-q} \tag{2.2b}$$

$$V_{\mathrm{th}} = \left(\frac{c_{\mathrm{i}}}{-q}\right)^{-1} N_{\mathrm{t}} \tag{2.2c}$$

where q_t is the amount of charge trapped in the deep trap level, N_t is the number of carriers trapped, and c_i is the capacitance of the gate insulator.

2.1.3 Current–Voltage Characteristics

As a semiconductor, p-type organic materials are often used than n-type semiconductors because of the high mobility and stability. The operation principles of p-type transistors

are described below.

At $V_{\mathrm{DS}} \approx 0$

When drain–source voltage $V_{\mathrm{DS}} \approx 0$ is applied under $V_{\mathrm{GS}} > V_{\mathrm{th}}$, carriers in the channel region drifts at the speed $v(< 0)$, which is in proportion to the electric field in the channel $E(< 0)$. The drain current I_{DS} is explained as

$$I_{\mathrm{DS}} = W q_{\mathrm{c}} v = W q_{\mathrm{c}} \mu E = -\mu \frac{W}{L} c_{\mathrm{i}} (V_{\mathrm{GS}} - V_{\mathrm{th}}) V_{\mathrm{DS}} = -\kappa (V_{\mathrm{GS}} - V_{\mathrm{th}}) V_{\mathrm{DS}} \tag{2.3}$$

where W is the channel width, L is the channel length, μ is the proportionality factor between E and v and called mobility. I_{DS} is rewritten in simple form with proportionally factor κ,

$$\kappa = \mu \frac{W}{L} c_{\mathrm{i}} \tag{2.4}$$

.

Linear Region

When higher V_{GS} is applied, the distribution of $V_{\mathrm{c}}(y)$ occurs in the channel between the edges of the source and the drain. Factor the distribution of q_{c} and the continuity of I_{DS}, I_{DS} are described as

$$I_{\mathrm{DS}} = -\kappa \left\{ (V_{\mathrm{GS}} - V_{\mathrm{th}}) V_{\mathrm{DS}} - \frac{1}{2} {V_{\mathrm{DS}}}^2 \right\} \tag{2.5}$$

.

The operation region that the I–V characteristics is explained by Eq. 2.5 is called linear region. Under small V_{DS}, V_{DS} is neglected and Eq. 2.5 becomes the same expression as Eq. 2.3.

Saturation Region

With $V_{\mathrm{DS}} < V_{\mathrm{GS}} - V_{\mathrm{th}}$, considering the continuity of I_{DS} and the the distribution of V_{CS}, I_{DS} is explained as

$$I_{\mathrm{DS}} = -\frac{\mu W c_{\mathrm{i}}}{2 y_{\mathrm{p}}} (V_{\mathrm{GS}} - V_{\mathrm{th}})^2 \approx -\frac{\kappa}{2} (V_{\mathrm{GS}} - V_{\mathrm{th}})^2 \tag{2.6}$$

.

The operation region that I_{DS} is explained as Eq. 2.6 is called saturation region.

I–V Characteristics

Typical I–V characteristics, or current–voltage characteristics, are shown in Fig. 2.3. The relation of I_{DS} and V_{GS} is called gate characteristic or transfer characteristic. The relation of I_{DS} and V_{DS} is called drain characteristic or output characteristic.

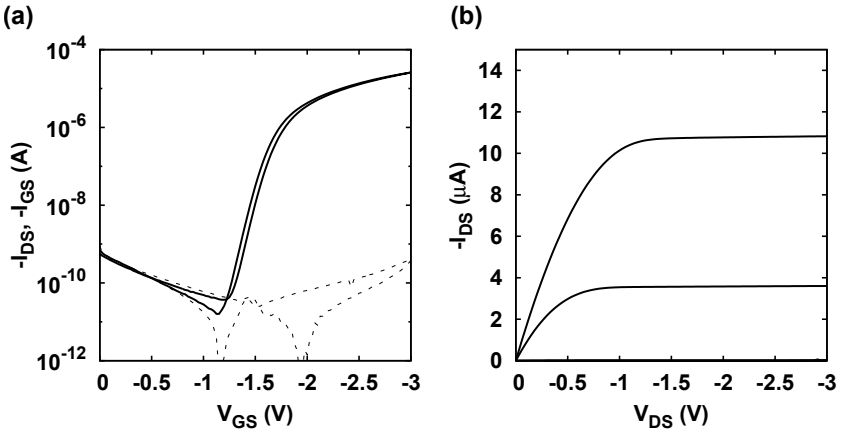

Figure 2.3: I–V characteristics of a p-type organic transistor. (a) Gate characteristic (solid line), leak current I_{GS} (dotted line) under $V_{\mathrm{DS}} = -2$ V. (b) Drain characteristic.

2.2 Organic Semiconductor

Organic semiconductors are the key element in organic transistors. In inorganic materials, semiconducting properties *i.e.*conduction band and valence band are formed by the existence of wave functions, bonding orbitals orbit splittings in single crystals. High mobilities like more than 1000 $\mathrm{cm}^2/\mathrm{V{\cdot}s}$ is achieved due to flawless, high-quality single crystals. On the other hand, in organic materials, the quality of single crystals are rather low. More defects exist in a singe crystal than inorganic materials. Therefore, wavefunctions like that of inorganic semiconductors hardly exist. Rather, highest occupied molecular orbital (HOMO) and lowest unoccupied molecular orbital (LUMO) act like conduction and valence bands.

The grain size, or the size of a single crystal, is small, normally a few nanometers, compared to the channel length, a few ten nanometers [21]. At the grain boundary, the bands are fractured and form barrier-like structure beside trap states. The conduction between molecules is called hopping conduction and is considered to cause lower mobility comparing to conduction in a molecule.

To achieve high mobility, highly π-extended aromatic compounds are essential to enable strong intermolecular overlap and enhance the carrier transport in the solid state. Among aromatic compounds, higher oligoacenes such as naphthacene and pentacene, shown in Fig 2.4, are reported to have high mobility of 0.7 $\mathrm{cm}^2/\mathrm{V{\cdot}s}$ [22] and 0.12 $\mathrm{cm}^2/\mathrm{V{\cdot}s}$ [23]. Beside the expanded π-framework, those oligoacenes are advantageous because a strong tendency to take herringbone packing which is suitable to construct two-dimensional electronic structure on the substrate when fabricated in thin-film-based devices. However, it is known that pentacene-based devices have poor properties in respect of stability and durability compared to inorganic devices.

Figure 2.4 shows frontier orbitals of oligoacenes. In the series of oligoacenes, the HOMO level becomes higher and the HOMO–LUMO gap becomes narrower as the num-

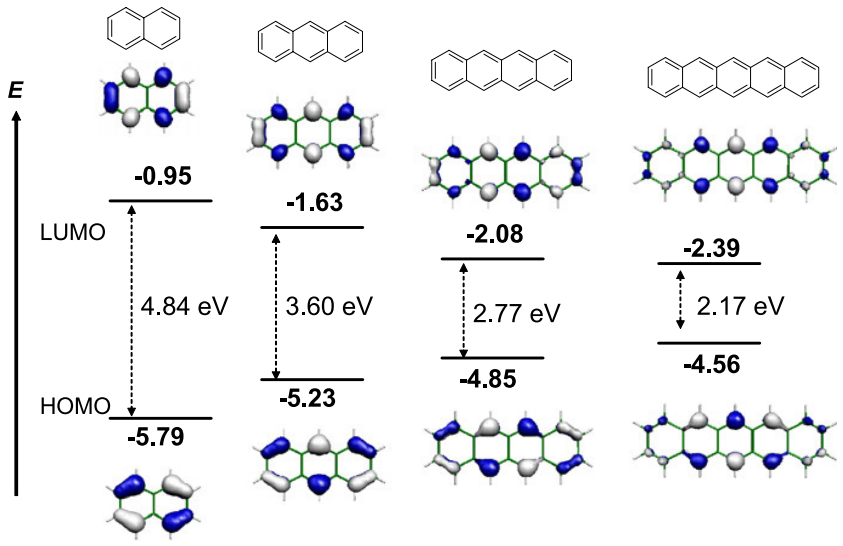

Figure 2.4: Calculated frontier orbitals of oligoacenes [24].

ber of benzene rings increases as seen in Fig. 2.4. From experimental and theoretical studies of electronic structures of organic molecules, the device stability originated from the relatively low-lying HOMO levels and the large HOMO–LUMO energy gaps of the heteroarenes High-lying HOMO level makes the molecule susceptible to air-oxidation in ambient conditions and narrow HOMO–LUMO gap will cause readily photo-induced excitation that may lead subsequent chemical reactions [24].

Based on above, Yamamoto et al. synthesized organic semiconductor dinaphtho[2,3-*b*:2',3'-*f*]thieno[3,2-*b*]thiophene(DNTT) [25]. HOMO–LUMO gap is 3.0 eV and HOMO level is 5.44 eV. The crystal structure of DNTT is shown in Fig. 2.6. The molecules are packed in herringbone packing and result in the two-dimensional molecular network. Thanks to the large expansion of π electron cloud, DNTT-based transistors achieve large mobility of 2.1–2.9 $cm^2/V{\cdot}s$ on Octadecyltrichrolosilane-treated Si/SiO_2 substrate. Typical mobility values of typical organic and inorganic semiconductors are shown in Table 2.1.

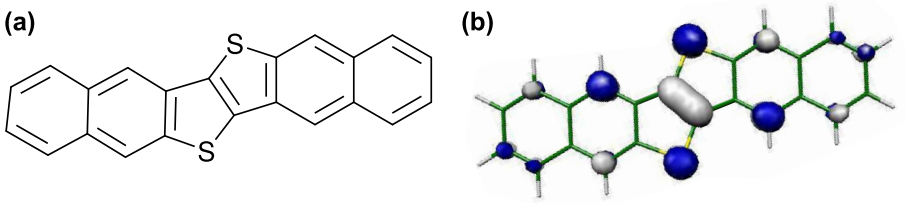

Figure 2.5: (a) Chemical structure and (b) calculated frontier orbitals of dinaphtho[2,3-*b*:2',3'-*f*]thieno[3,2-*b*]thiophene(DNTT) [25].

Pentacene-based TFTs achieved higher performance than amorphous silicon TFTs by Klauk et al. in 2007 [3]. However, there still exists many problems such as energy

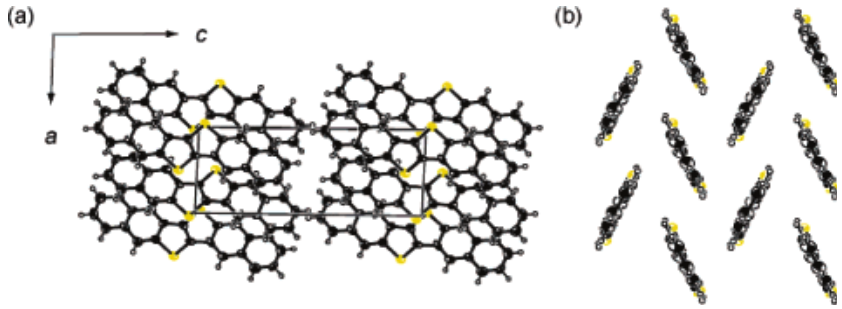

Figure 2.6: (a) Crystal structure *b*-axis projection and (b) herringbone packing in the layered structure of DNTT [25].

Table 2.1: Typical mobility value of organic and inorganic semiconductors.

Material	Mobility (cm^2/V·s)	
Si	1900	(electron)
Ge	3800	(electron)
Pentacene [22]	0.7	(hole)
DNTT [25]	1–3	(hole)

consumption, stability and durability. Now many efforts are done in search for more better organic semiconductors.

2.3 Self-Assembled Monolayers

SAMs are ordered molecular assemblies formed by the adsorption of an active surfactant on a solid surface and are commonly used to modify the surface of gate dielectrics in transistors in the field of electronics. A molecule that forms monolayer by self-assembly has three parts: an anchor group, a spacer group, and a terminal functional group.

The anchor group (head group) is responsible for the adsorption of the molecule by forming chemical bonds to the adsorbent surface. The terminal functional group (tail group) determines the properties of SAM surface. The group between the anchor and terminal groups (spacer group) normally consists of a long alkyl chain with 10 to 18 methylene group (–CH_2–). The spacer group determines the intermolecular interactions and promotes the ordering and orientation of the molecules within the monolayer. It might also influence the film formation, growth process, and subsequently electric properties.

SAM molecules are generally grouped according to the head group: the thiol group (–SH) is applicable to especially gold surfaces, whereas phosphonic [–$PO(OH)_2$], sulfonic [–$SO_2(OH)$], silanol [–$Si(OR)_3$], and silyl (–SiR_3) groups are more suitable for adsorption on oxide materials such as Al/AlO_2, Ti/TiO_2 and so on [26].

SAMs are formed by simple process; conventionally by dipping the surface-activated substrate to the solution of the molecules (Fig. 2.7). When the substrate is dipped, the head group of the SAM molecules are adsorbed to the surface of the substrate, in

most cases very hydrophobic. With the intermolecular force, the molecules assemble spontaneously and form a two-dimensional layer. The tail group of the molecule is often hydrophobic, therefore the formation of additional layer is unlikely to occur.

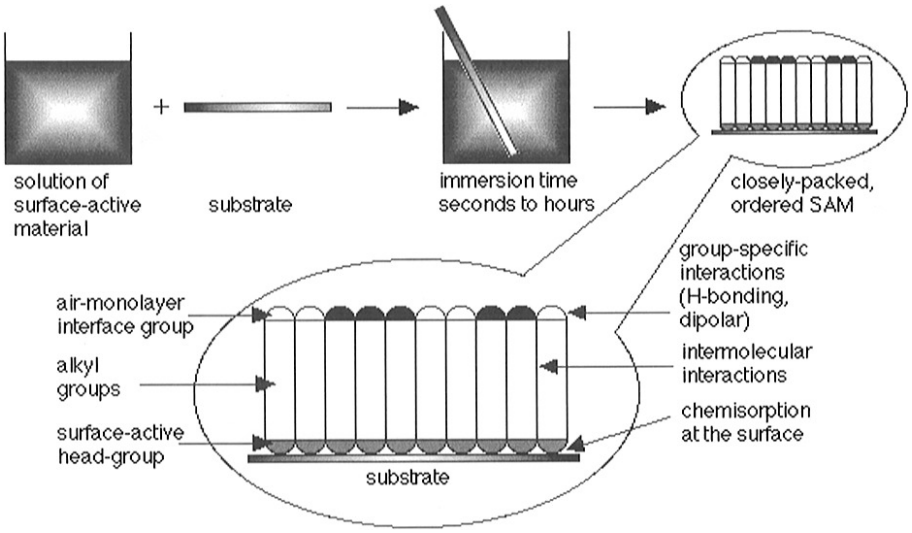

Figure 2.7: Schematics of the SAM formation. Substrates are simply immersed into a solution of the surface-active material. The driving force for the spontaneous formation of the 2D assembly includes chemical bond formation of molecules with the surface and intermolecular interactions.

In electric devices, the surface modification by SAMs has many advantages. First, SAM is tightly packed and reduces leak current. Second, SAM is very thin, the thickness is approximately equivalent to the length of the molecule, 1–2 μm. Therefore, a thick insulator layer to reduce leak current and improve on/off ratio is not necessary and the threshold voltage itself is greatly reduced. Third, the SAM improves the surface smoothness of the layer underneath and, particularly in bottom-gate geometry, high mobility is realized.

Klauk et al. demonstrated the insulating ability of SAMs and high mobility of pentacene-based p-type OTFTs which are operated at lower driving voltage and realize higher performance than amorphous silicon TFTs [27]. As shown in Fig. 2.8, phosphonic acid-based SAM shows the smallest leakage current density among without SAM (AlO_x only) and silane-based SAM. In this work, the combination of phosphonic acid-based SAMs and aluminium oxide is adopted as the gate insulator.

2.4 Methods for Threshold Voltage Control

2.4.1 In-Process Control

Control of the threshold voltage is one of the methods to enhance device properties and to reduce energy consumption. Though the characteristics of OTFTs are far different from

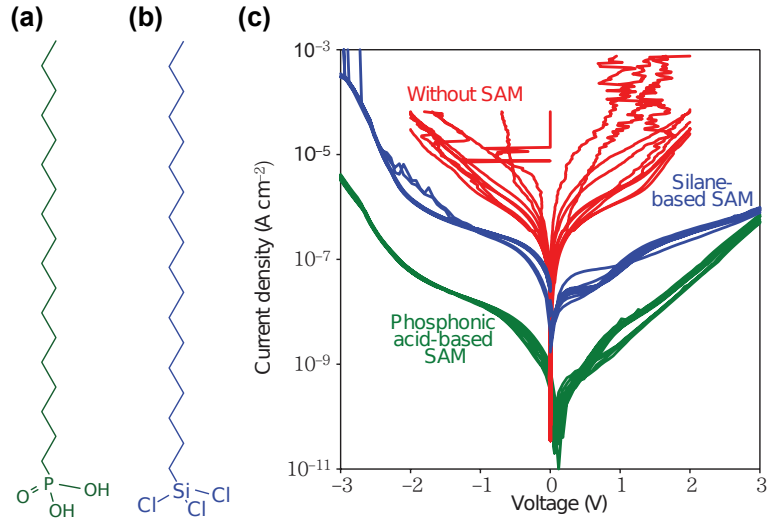

Figure 2.8: (a) Chemical structure of *n*-octadecylphosphonic acid. (b) Chemical structure of *n*-octadecyltrichlorosilane. (c) Leakage current density as a function of applied voltage. [27].

inorganic TFTs, many researches are done to increase the device controllability until present.

Doping

Theoretically, the threshold voltage of an organic transistor $V_{\text{th}}$is defined as Eq. 2.2c. Since the organic semiconductors in OTFTs have more defects than inorganic semiconductors, the number of traps are larger than inorganic semiconductors, even in single crystal OTFTs, including traps at the interface of insulator and semiconductor. For polycrystalline or amorphous crystals, the continuity of HOMO and LUMO levels are fractured at the grain boundaries, producing more trap states. Trap density in organic crystals is governed by many uncontrollable factors, therefore it is very difficult to control threshold voltage by doping, as is widely used in inorganic transistors.

Still, doping is one of approaches to control the threshold voltage of organic transistors. Abe et al. deposited an organic acceptor layer of tetrafluoro-tetracyanoquinodimethane (F_4TCNQ), which provides mobile holes, on pentacene channel layer to realize doping [28]. The result by doping is shown in Fig. 2.9. Under the source–drain voltage of -1.0 V and the gate voltage of 50 V, the threshold voltage shifted 50 V according to the proportion of doped area to total channel area d/l.

However, in general, dopant molecules are known to unstable in the air. Also, when the dopants are deposited on channel layer, the dopant molecules diffuse into channel layer. The diffused molecules reduces the contact resistance but reduces mobility. Therefore it is not appropriate to apply doping as a V_{th}control method,

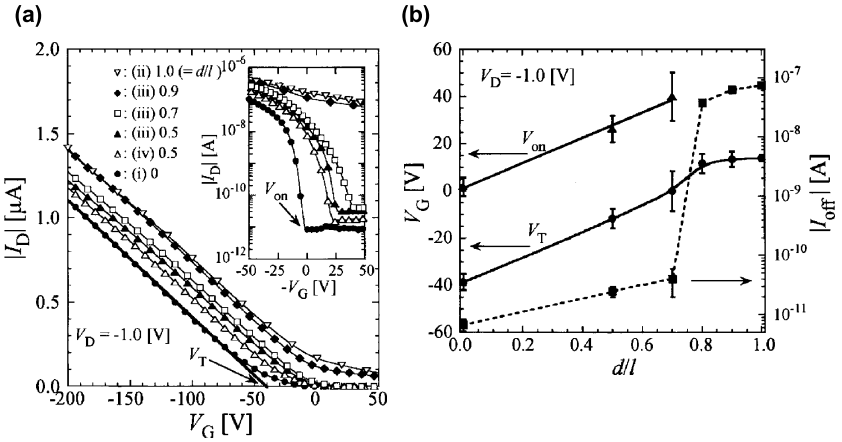

Figure 2.9: (a) Transfer curves of top-gate OTFTs with various doping geometries. The inset is semilogarithmic plot of transfer curves. (b) Shift of threshold voltage $V_{\rm th}$(closed circle), turn-on voltage $V_{\rm on}$ (closed triangle), and off-current $I_{\rm off}$ (closed square), plotted as a function of d/l, the proportion of doped area to total channel area [28].

Gate Dielectric Thickness Control

Other approach is to control the thickness of the gate insulator. Since the capacitance of the gate dielectric c_i is defined as Eq. (2.1b), the threshold voltage control is achieved by controlling either the permittance of the insulator ϵ_i or the thickness d. The threshold voltage control by the thickness of the gate insulator d is demonstrated with the gate insulator materials of cross-linked organic insulating polymers and self-assembled monolayers (SAMs). Besides the simple and precise control, those methods realize smooth surface of the channel-insulator interface, which decreases the trap state at the interface and consequently increase the overall mobility.

Kawaguchi et al. formed cross-linked poly(cyanoethylacrylate) (PCA) and the cross-linking agent blocked polyisocyanate as the gate dielectrics by spin coating on Al/AlO_x insulator and fabricated copper phthalocyanine (CuPc)-based OTFTs [29]. By changing the concentration of solvent and spin rate and time of spin coating, the thickness of the gate dielectric with continuous value of thickness 60–600 nm was obtained. The result is shown in Fig. 2.10.

Fukuda et al. formed SAMs of phosphonic acids with various alkyl chain lengths on AlO_x gate insulator [21]. According to the alkyl chain length, the threshold voltage shifted, however, this methods strongly depends on the material. Therefore, continuous control of the threshold voltage is difficult.

Surface Modification of Gate Dielectric

Surface modification is a very effective method to control the threshold voltage in organic transistors. By modifying the surface of the gate insulator with electron-donating or withdrawing materials, the threshold voltage shifts drastically.

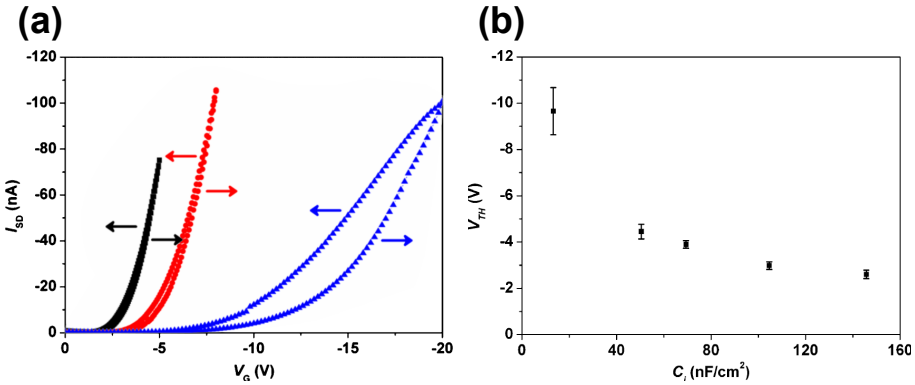

Figure 2.10: (a) Transfer curves of OTFTs with the various insulator thicknesses. The capacitance value of each hybrid insulator thickness is 146 nF/cm^2 (black), 69 nF/cm^2 (red), and 13 nF/cm^2 (blue) respectively. (b) Threshold voltage as a function of the capacitance of gate dielectrics in the forward sweep [29].

On Si/SiO_2 substrate, SAMs of hexamethyldisilazane (HDMS) [30], organosilane [31], and octadecyltrichrolosilane [32] were demonstrated to shift threshold voltages. On Al/AlO_x gate insulator, fluoroalkyl phosphonic acid has a function to draw electrons, and shifts the threshold voltage to positive direction. Kraft et al. fabricated pentacene-based p-type transistors and F_{16}CuPc-based n-type transistors on Al/AlO_x gate dielectrics modified with dodecylphosphonic acid (HC12-PA) and $1H,1H,2H,2H$-perfluorododecylphosphonic acid (FC12-PA) [17]. Under low driving voltage of 2–3 V, FC12-PA SAM shifted the threshold voltages to 1.0–1.2 V in positive direction.

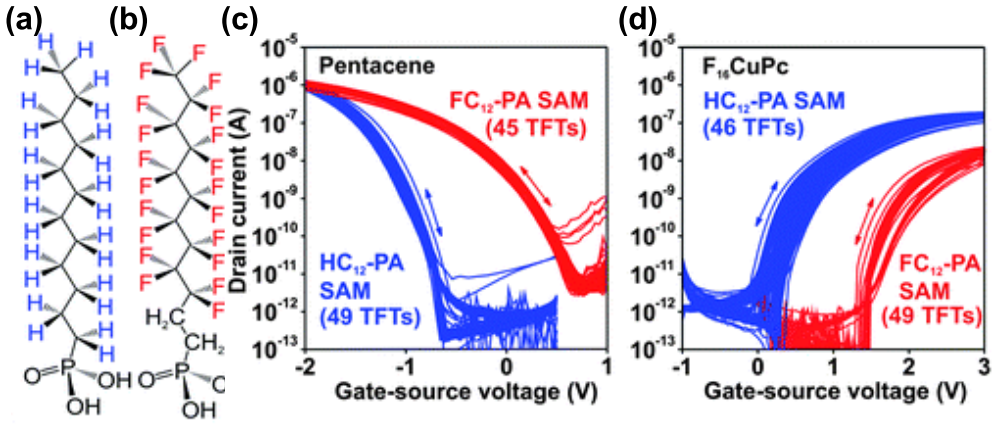

Figure 2.11: (a) Chemical structure of dodecylphosphonic acid (HC12-PA). (b) Chemical structure of $1H,1H,2H,2H$-perfluorododecylphosphonic acid (FC12-PA). Transfer curves of (c) pentacene-based p-type OTFTs and (d) F_{16}CuPc-based n-type OTFTs. In both OTFTs, the surface of Al/AlO_x gate insulator was modified with either HC12-PA (blue) or FC12-PA (blue) and the threshold voltage was shifted to 1.0–1.2 V to positive direction by fluorinated SAMs under low driving voltage of 2–3 V [17].

To determine the value of the threshold voltage continuously, Zschieschang et al.

mixed alkyl-phosphonic acid SAMs and fluorinated SAMs [33, 18]. The shift of the threshold voltage and the switching voltage is linear to the atomic concentration of fluorine in SAMs (Fig. 2.12).

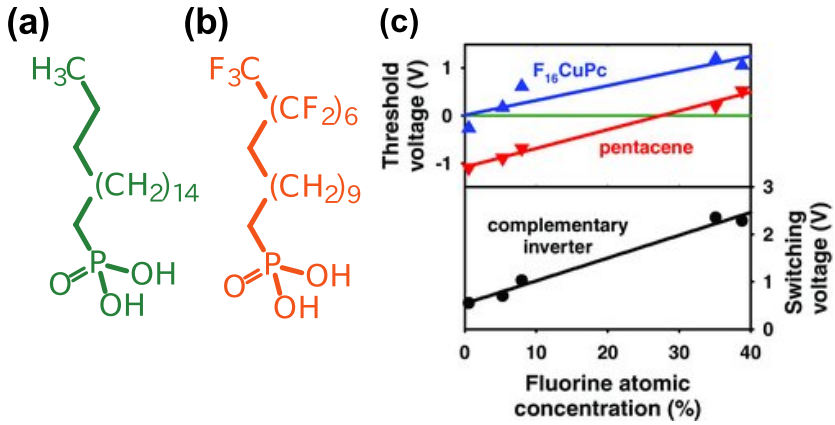

Figure 2.12: (a) Chemical structure of octadecyl-phosphonic acid. (b) Chemical structure of pentadeclfluoro-octadecylphosphonic acid. (c) Threshold voltages of OTFTs and switching voltages of CMOS inverters as a function of the concentration of fluorine atomic concentration in the SAM gate dielectric. [18].

2.4.2 Post-Process Control

Especially in large-scale fabrication such as active transistor matrix and memory matrix, the variation in fabricated TFTs is critical problem, since the variation decrease the whole device performance. After fabrication, by measuring each TFT, variation in the TFT characteristics is revealed. It is highly favorable for devices that the threshold voltages are tunable after fabrication.

Double-Gate Structure

Double-gate structure is demonstrated by Iba et al. [34, 35] In double-gate structure, additional top-gate electrode and insulator is formed on a transistor with bottom-gate, top-contact geometry (Fig. 2.13 (a)). By applying bias to the top-gate electrode, the potential of the channel is controlled and the threshold voltage is shifted (Fig. 2.13 (b)).

This method enables the control of the threshold voltage almost linearly (Fig. 2.13 (c)), however, the fabrication process needs additional process steps of the formation of parylene and top-gate electrodes. Moreover, large driving voltage and gate–source voltage of -40 V is necessary, which leads to large energy consumption.

Floating Gate Structure

The control of the threshold voltage with lower driving voltage is demonstrated with floating-gate structure [36]. The structure is shown in Fig. 2.14 (a). In the gate insulator,

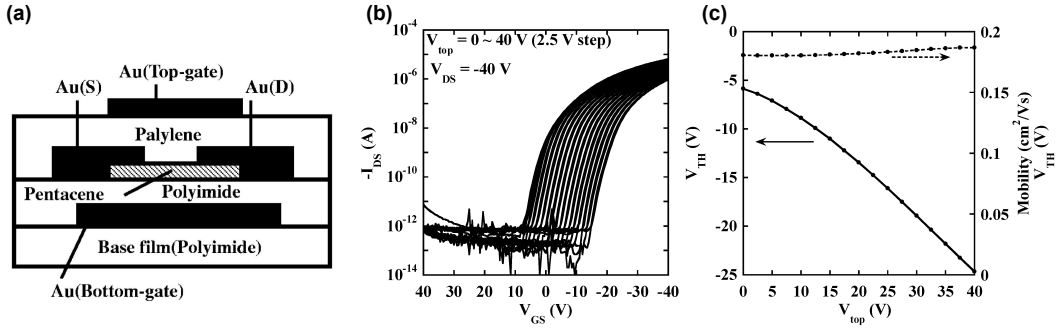

Figure 2.13: (a) Schematic of a double-gate structure. (b) Transfer characteristics of p-type organic transistor with double-gate structure. (c) Mobility and threshold voltage change in p-type organic transistors with double-gate structure [35].

Table 2.2: Summary of methods to control threshold voltages.

Method	Process	Precise Control	Stability	Mobility ($cm^2/V{\cdot}s$)	V_{GS}, V_{DS} (V)	Spatial Control
Doping [28]	Vacuum	Hard	Unstable	1	50	Easy
Dielectric thickness [29]	Solution	Stable	Easy	1.7×10^{-3}	5	No
Surface modification [17, 18, 33]	Solution	Stable	Easy	1	3	No

floating gate is embedded. When the dielectric is sufficiently thin, electric charge penetrate through the dielectric and is brought onto the floating by quantum tunneling or thermal emission by applying a large program voltage between the control gate and the source contact. Charging the floating gate shifts the threshold voltage (Fig. 2.14 (b), (c)). Also, the floating gate is isolated and the charge remains on the floating gate without applying any voltage.

The methods above are summarized in Table. 2.2 in the aspects of process simpleness, control preciseness, device mobility, stability, energy consumption *i.e.*driving voltage and threshold voltage, and spatial controllability.

For certain applications it is highly desirable to have TFTs with different threshold voltages in specific locations on the same substrate. SAMs are generally formed by dipping the entire substrate into a solution of the molecules, so that all TFTs on the substrate end up having the same threshold voltage [21, 31, 32, 18]. As for spin coating method,

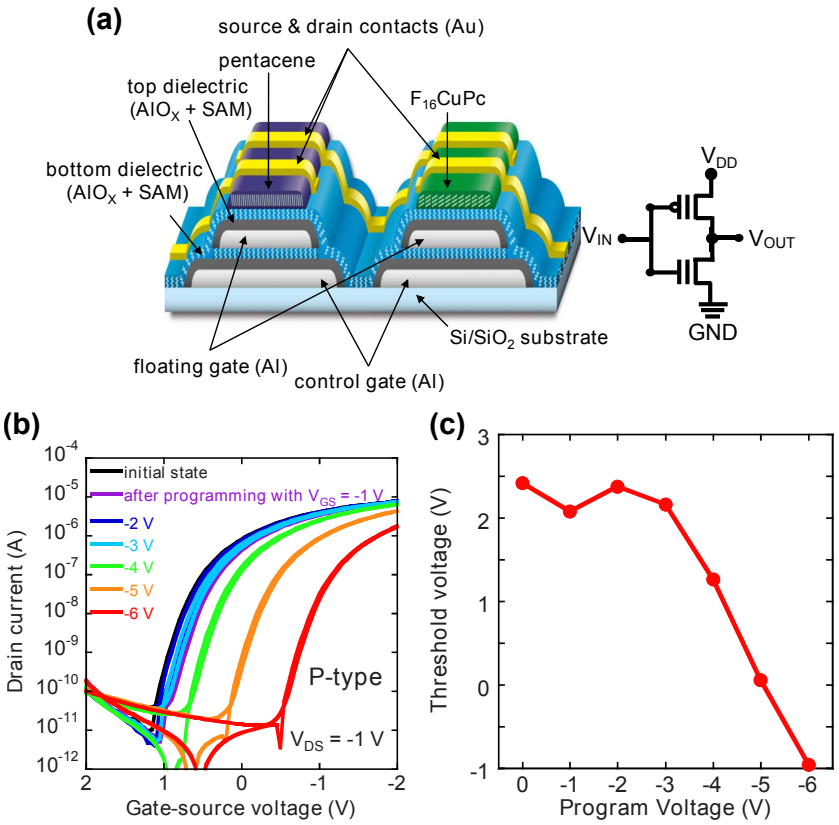

Figure 2.14: (a) Schematic cross-section and circuit diagram of the floating-gate complementary inverter. (b) Transfer characteristics of pentacene TFTs with various program voltages ranging from -1 to -6 V. (c) Threshold voltage of the p-channel TFTs as a function of the program voltage applied prior to the measurement [36].

polymer gate dielectrics with uniform thickness is formed. Lithography is one of the methods to form different thickness of polymer layers on one substrate, however, the number of process steps is increased by lithography.

Chapter 3

Device Fabrication

3.1 Device Structure

The schematic view and an optical microscopic image of the fabricated transistor are shown in Fig. 3.1(a) and (b). Transistors in this work have top-contact bottom-gate geometry. The schematic overall view is shown in Fig. 3.1(c). One sample have 20 transistors (Al/AlO_x/SAM/DNTT/Au) and 5 capacitors (Al/AlO_x/SAM/Au, without semiconductor).

Schematics of the fabrication process is shown in Fig. 3.1(d). The Al gate electrodes with a thickness of 30 nm were evaporated through a shadow mask onto a Si substrate with a 500 nm thick oxidized surface. The surface of the electrode was oxidized by plasma (200 W, 30 s) to form a thin, dense AlO_x layer. The gate dielectrics of SAM, tetradecylphosphonic acid (HC14-PA), pentadecylfluoro-octadecylphosphonic acid (FC18-PA), or perfluorooctyl phosphonic acid (FC8-PA), were then formed onto Al/AlO_x stack by either stamping or dipping, then rinsed with pure 2-propanol [21]. The last step in both the stamping and dipping process was to bake the substrate in an oven at 100 °C for 10 min. A 30 nm thick layer of organic semiconductor dinaphtho[2,3-*b*:2',3'-*f*]thieno[3,2-*b*]thiophene (DNTT) [25] was evaporated at room temperature. Finally, the source and drain electrodes with a channel length of 40 nm were evaporated.

The chemical structures of SAMs and DNTT is shown in Fig. 3.2.

3.2 Spatial Formation of SAMs

3.2.1 Soft lithography

As described in Section 2.4, for certain applications spatial control of the threshold voltages is necessary. Conventionally, SAM is formed by dipping (Fig. 2.7), however, this methods forms uniform layer overall the substrate, therefore the all TFTs on the substrate have the same threshold voltage. To solve this problem, soft lithography technique is adopted in this work.

Soft lithography is one of micro- or nano-scale patterning technique using printing,

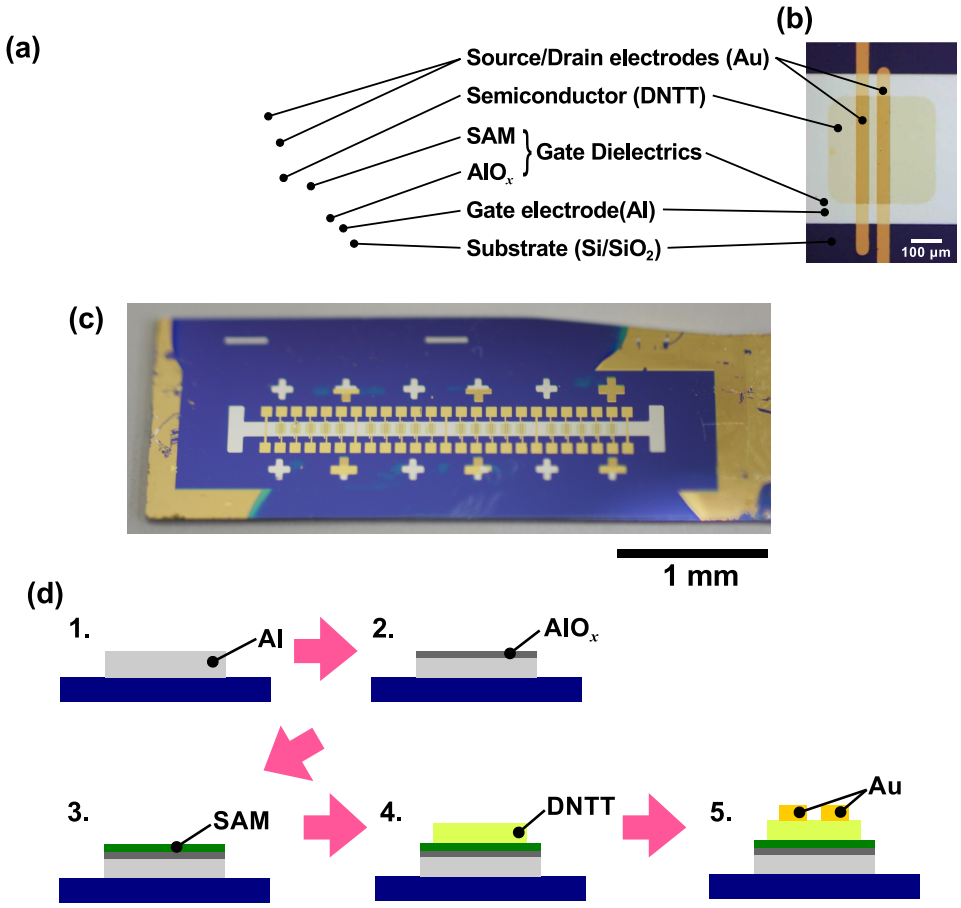

Figure 3.1: (a) A schematic view and (b) an optical microscopic image of the fabricated transistor with top-contact, bottom-gate geometry. (c) A completed device with 20 transistors and 5 capacitors. (d) Schematics of the fabrication process of the transistor.

molding, and embossing, named for its use of soft, elastomeric elements (polydimethylsiloxane (PDMS) is commonly used), and now it is widely applied for bioelectronics and microelectronics.

Compared to conventional photolithography, soft lithography has many advantages: First, soft lithography is an inexpensive process, which is performed outside of the clean room. Second, soft lithography does not need photomasks for patterning. This feature greatly reduces the time and cost. Third, soft lithography provides large variety of materials and surface chemistry and mechanical structure, such as curved or non-planer substrates [37].

Soft lithography was first used to transfer self-assembled monolayers to form resist layer on gold, supported by silicon substrate, for selective etching [38, 19] (Fig. 3.3), then applied for surface patterning for biosensors [39], which process is described as microcontact printing. Subsequently methods called replica molding, solvent assisted micro-molding were developed, and today soft lithography techniques are used for two-dimensional and three-dimensional structure transfer [40] and direct patterning of mam-

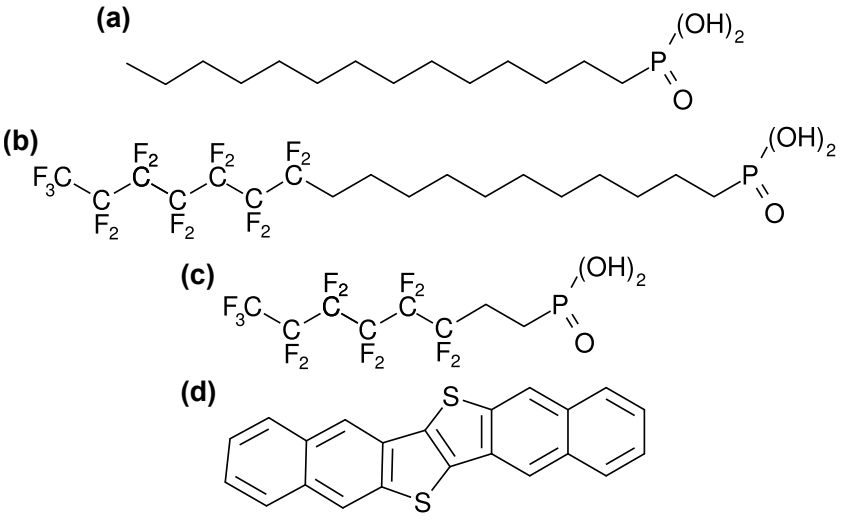

Figure 3.2: Chemical structures of SAMs and organic semiconductor used in this work. (a) Tetradecylphosphonic acid (HC14-PA); (b) Pentadecylfluoro-octadecylphosphonic acid (FC18-PA); (c) Perfluorooctyl phosphonic acid (FC8-PA); (d) Dinaphtho[2,3-*b*:2',3'-*f*]thieno[3,2-*b*]thiophene (DNTT).

malian cell on tissue [41].

In principle, microcontact printing method can accomplish the area-selective formation of SAMs, besides providing a wide patterning range of surface modification materials. However, to our knowledge, this possibility has not been exploited so far.

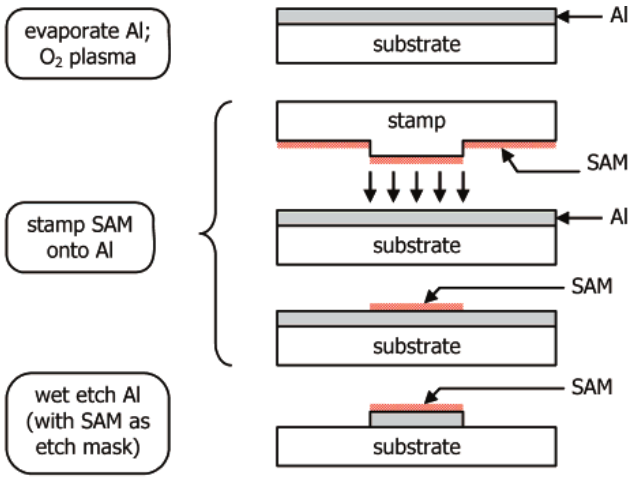

Figure 3.3: Process flow of the etching, masked with microcontact-printed phosphonic acid self-assembled monolayer [19].

3.2.2 SAM Formation Process

SAMs were formed by either stamping or conventional dipping. The schematics of the processes are shown in Fig 3.4.

In the stamping process, SAMs were transferred to the substrate from a polydimethylsiloxane (PDMS) elastomer [19, 42]. PDMS stamps were prepared by using Sylgard®184 Silicone Elastomer Kit.

First, polymer base and the curing agent were mixed in a ratio of 10 parts base to one part curing agent by weight. During mixing the liquid, a gradual increase in viscosity occurs and the air is trapped in the liquid as bubbles. The bubbles reduces the flatness of the surface of PDMS stamp. To release the air bubbles, mixed liquid was put into a vacuum desiccator and left under low pressure for about 30 minutes. After all air is released, the liquid was poured in the mold on Si/SiO_2 substrate and baked in an oven for 1 hour at 60 °C. Stamps were then peeled off from the Si/SiO_2 substrate and rinsed in pure 2-propanol and dried in an oven at 60 °C.

To transfer the SAM molecules, PDMS stamp was first dipped into 2-propanol solution of 1 mmol/ℓeither HC14-PA, FC18-PA, or FC8-PA solution for 5 min and then placed onto the $Si/Al/AlO_x$ surface for 10 min to allow a molecular monolayer to self-assemble. In the dipping process, the substrate was immersed in a 2-propanol solution of HC14-PA, FC18-PA, or FC8-PA solution for more than 13 hours.

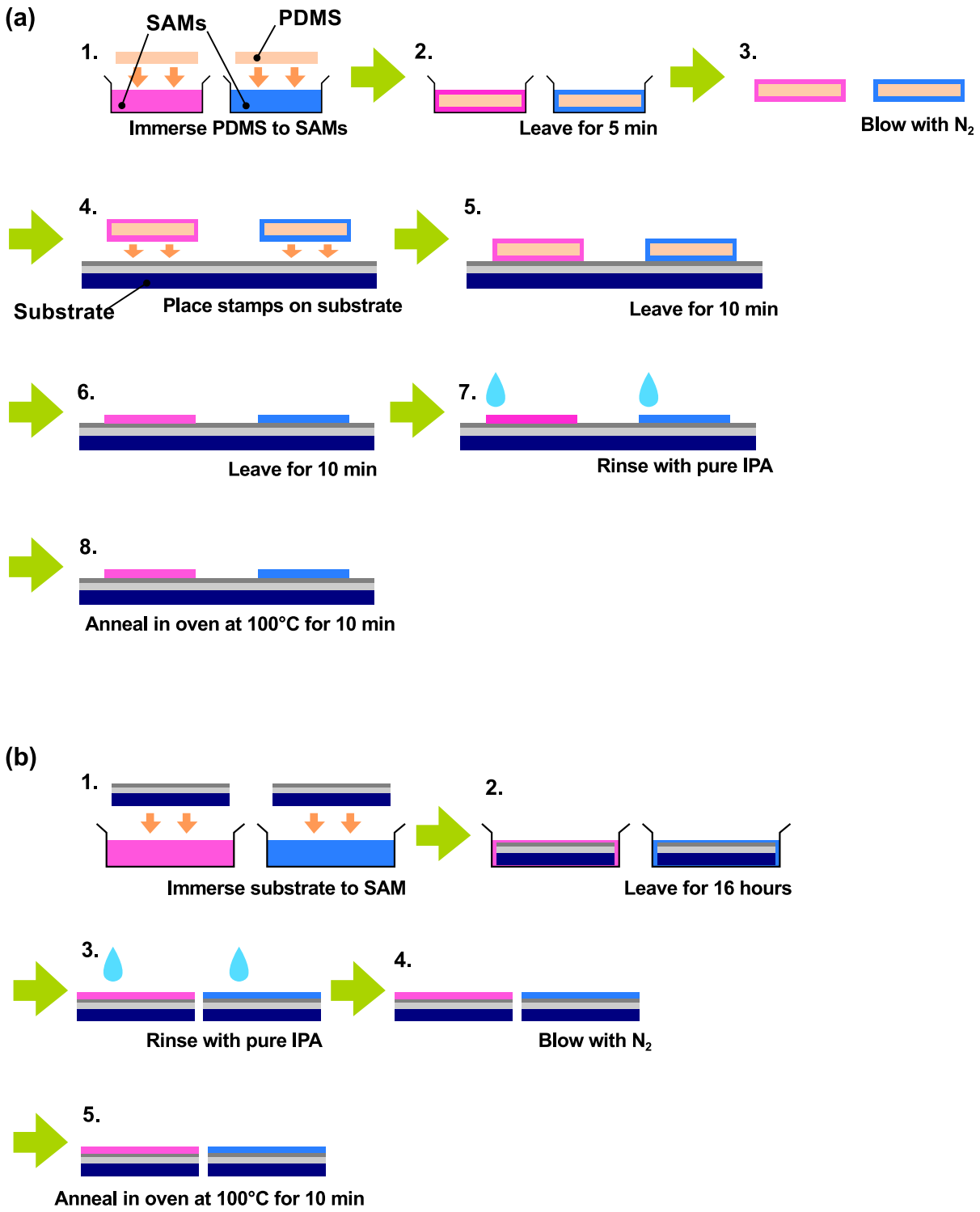

Figure 3.4: Process flow of SAM formation by (a) stamping and (b) conventional dipping.

Chapter 4

Characterization Methods

4.1 Electric Properties

For thin film transistors, the threshold voltage and the mobility are most important properties to evaluate the quality.

For inorganic transistors, the threshold voltage is defined as the voltage which induces the inversion layer onto the interface of the channel layer and the gate insulator. As for organic transistors, there are many definitions of the threshold voltage, since the function mechanism of organic transistors is fundamentally different from the inorganic transistors. Generally, $V_{\mathrm{th}}$is defined by conforming equations such as Eq. 2.2c to current–voltage characteristics. There are many definitions for mobility as well, such as intrinsic mobility, Hall mobility, field-effect mobility, effective mobility.

In actual devices, the equation of current-voltage characteristics in the saturated region of inorganic transistors Eq. 2.6 well explains the carrier transportation phenomena in organic transistors. In this work, the threshold the voltage and field-effect mobility are calculated by fitting transfer curves to Eq. 2.6 in the saturation region by least-square method as shown in Fig. 4.1.

4.2 Contact Angle

The determination of solid–vapor (γ_{sv}) and solid–liquid (γ_{sl}) interfacial tensions is important in a wide range of problems in pure applied science. Contact angle measurement is a commonly used method to determine surface tensions. In this work, contact angle measurement is applied to confirm the formation of SAMs on AlO_x layer. The formation of SAMs is easily interpreted from the contact angle, since the surface of the AlO_x is very hydrophilic while the surface of the SAMs, or the assembled tail groups of the SAM molecules, is very hydrophobic, as described in Section 2.3.

The relation between the solid surface tensions and contact angles has been recognized by Young[43]. The contact angle of a liquid drop on a solid surface is defined by mechanical equilibrium on the drop under the action of three interfacial tensions 4.2: solid–vapor,

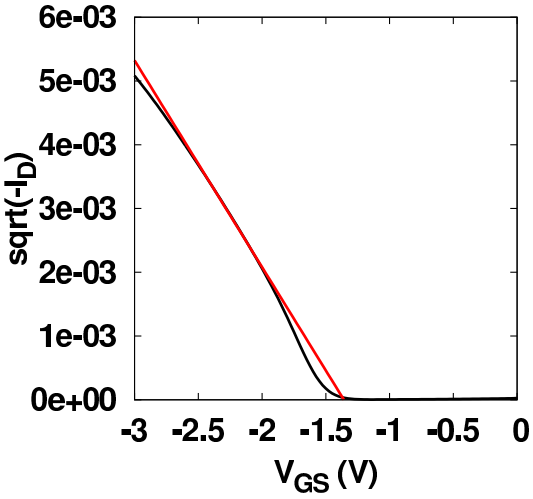

Figure 4.1: Calculation of the threshold voltage and the field-effect mobility in the saturation region. By the slope of the line (red) to the transfer curve (black), the mobility μ is calculated. X-intercept is the threshold voltage V_{th}.

γ_{sv}, solid–liquid, γ_{sl}, and liquid–vapor, γ_{lv}. This equilibrium relation is known as Young's equation:

$$\gamma_{lv} \cos\theta_Y = \gamma_{sv} - \gamma_{sl} \tag{4.1}$$

where θ_Y is the Young contact angle.

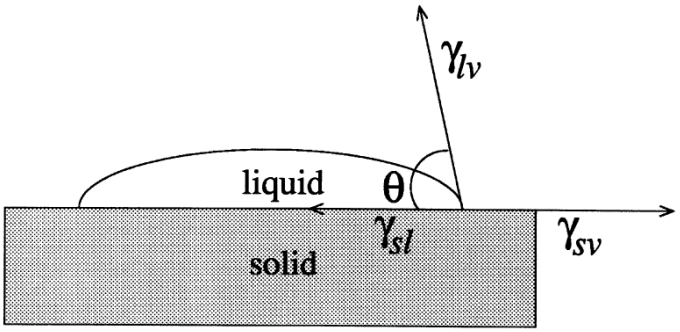

Figure 4.2: Schematic of a sessile-drop contact angle system [44].

In this work, water droplets with the volume of about 1 $\mu\ell$ were dropped on sample surfaces. $\theta/2$ method was applied to extract the contact angle θ 4.3.

4.3 Near-Edge X-ray Absorption Fine Structure (NEXAFS)

The near-edge X-ray absorption fine structure or, for short, NEXAFS is one of the optical measurement techniques for elucidating especially low-Zmolecule structures bonded in thin films, developed since the 1980s. In the measurement, the incident X-ray energy is scanned in the region close to core absorption edge and absorption intensity is measured.

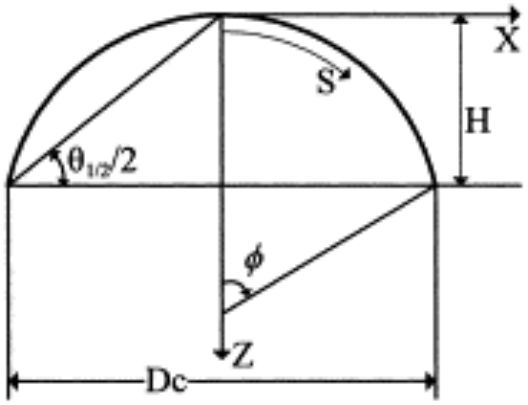

Figure 4.3: Coordinate system of sessile drop and the $\theta/2$ method [45].

NEXAFS selects a specific atomic species through its K-edge and probes its bonds to intra-molecular and, to lesser degree, extra-molecular (*i.e.* surface atoms) neighbors. Among the capabilities are: the ability to detect the presence of specific bonds in molecules (e.g., C–C, C=C, C≡C, and C–H bonds in hydrocarbons), the determination of the lengths of these intra-molecular bonds and the derivation of the precise orientation of molecules and functional groups on surfaces or in solids.

4.3.1 Electron Excitation and Intensity Measurement[46]

Schematic of photon-absorption and relaxation processes are shown in Figure 4.4(a). By the incident photon, an electron at the core level excites to an unoccupied states. Then recombination occurs at the core hole, radiative or non-radiative. Radiative type produces fluorescent x-ray, while non-radiative type produces an Auger electron. This primary Auger electron is highly surface sensitive and is measured in NEXAFS measurement.

The most common methods to record the intensity of the excitation, *i.e.*NEXAFS spectra are transmission and electron yield measurements. While total transmission measurement requires very thin foils of samples, the electron yield measurement, often called total electron yield (TEY) detection, can be used for conventional samples. The absorbed x-ray intensity is not measured directly in TEY measurements, but rather the photoelectrons created by the absorbed X-rays.

The primary Auger electron produced by incident X-ray is the direct measurement of X-ray absorption process and is used in Auger electorn yield (AEY) measurements. As the primary Auger electrons leave the sample, they create scattered secondary electrons (Fig. 4.4(b)). which dominate the TEY intensity. The TEY cascade involves several scattering events and originates from an average depth, the electron sampling depth L. Electrons created deeper in the sample lose too much energy to overcome the workfunction of the sample and therefore do not contribute to TEY. The sampling depth L in TEY measurements is typically a few nanometers, while it is often less than 1 nm for AEY measurements. In partial electron yield (PEY) detection, electrons of kinetic energy

larger than a threshold energy E_{P} are detected.

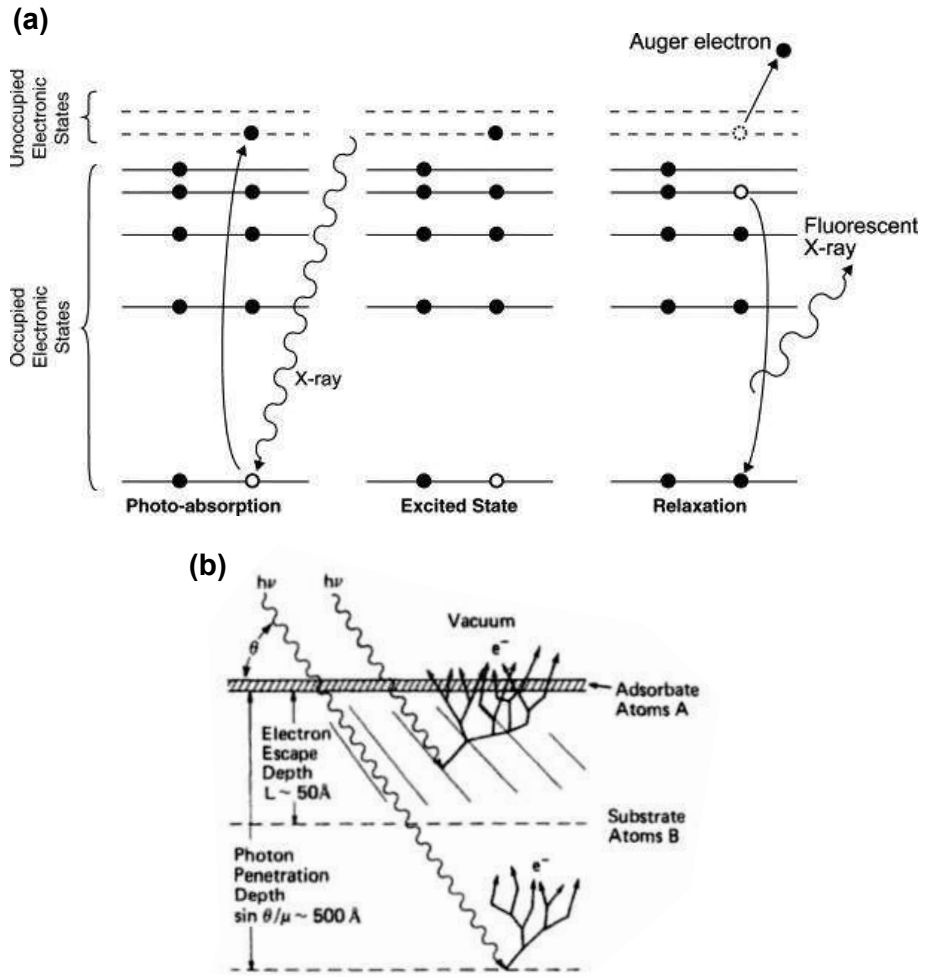

Figure 4.4: (a) Schematic of the photon-absorption and relaxation processes in a NEXAFS measurement. The incident photon excites an electron from a core level to an unoccupied, anti-bonding level. This excited state is unstable and the electron relaxes to eject either a fluorescent photon or an Auger electron [47]. (b) Photoabsorption and electron production in a single consisting of substrate atoms B and an absorbate layer A. Only electrons created within a depth L from the surface contributes to the measured electron yield signal. Electrons originating from layer A constitute the NEXAFS signal; those from layer B give rise to unwanted background [46].

4.3.2 The Angular Dependence of Resonance Intensities [46]

The intensity of the X-ray absorption, or resonance, *i.e.* the electron transition is determined by the angle of the polarized X-ray incident. The dependence of resonance is explained by X-ray absorption rate, or cross section σ_{x}as

$$I_{if} \propto \sigma_{\mathrm{x}} \tag{4.2}$$

where $\sigma_{\mathrm{x}}$is

$$\sigma_{\mathrm{x}} = \frac{4\pi^2\hbar^2}{m^2}\frac{e^2}{\hbar c}\frac{1}{\hbar\omega}\left|\langle f\left|\boldsymbol{e}\cdot\boldsymbol{p}\right|i\rangle\right|^2\mathcal{Q}_f(\mathrm{E}) \tag{4.3}$$

where $\boldsymbol{e}$ in the braket is the electron field of the polarized incident, $\boldsymbol{p}$ is linear momentum operator of electron, $\mathcal{Q}_{\{}$ is the energy density of the final state. The dipole matrix element $\boldsymbol{p}$ is used to determine the orientation of the molecule, since the NEXAFS spectrum depends on the polarized incident, and expressed in other form as

$$\boldsymbol{p} = m\boldsymbol{v} = i\hbar\nabla = \frac{im(E_f - E_i)}{\hbar}\boldsymbol{r} = \frac{i\hbar}{E_f - E_i}\nabla V \tag{4.4}$$

where V is the potential energy of electron-nuclear attraction and electron-electron repulsion. From Equations 4.3 and 4.4 the dependence of the resonance intensity is obtained and Eq. 4.2 is rewritten as

$$I_{if} \propto \left|\langle f\left|\boldsymbol{e}\cdot\boldsymbol{p}\right|i\rangle\right|^2 \propto \left|\boldsymbol{e}\cdot\langle f\left|\boldsymbol{r}\right|i\rangle\right|^2 \tag{4.5}$$

. $\boldsymbol{e}\cdot\langle f\left|\boldsymbol{r}\right|i\rangle$ is defined as the transition dipole moment (TDM) associated with a transition between the initial and the final states.

In NEXAFS measurement, an electron excites from initial state K-shell *1s* to final states π^* and σ^*, therefore the initial and the final states are rewritten as Eq. 4.6.

$$\begin{aligned} |f\rangle &= a\left|2s\right\rangle + b\left|2p_x\right\rangle + c\left|2p_y\right\rangle + d\left|2p_z\right\rangle \\ &= aR_{2s}(\boldsymbol{r}) + R_{2p}(\boldsymbol{r})(b\sin\theta\cos\phi + c\sin\theta\sin\phi + d\cos\theta) \qquad (4.6a) \\ |i\rangle &= R_{1s}(\boldsymbol{r}) \qquad (4.6b) \end{aligned}$$

TDM is explained by representing $\boldsymbol{r}$ in polar coordinates $\boldsymbol{r} = r(\sin\theta\cos\phi\boldsymbol{e}_x + \cos\theta\cos\phi\boldsymbol{e}_y + \cos\theta\boldsymbol{e}_z)$,

$$\langle f\left|\boldsymbol{r}\right|i\rangle = R\frac{4\pi}{3}(b\boldsymbol{e}_x + c\boldsymbol{e}_y + d\boldsymbol{e}_z) \tag{4.7}$$

where R is radial dipole matrix element

$$R = \int R_{1s}(\boldsymbol{r})R_{2p}\boldsymbol{r}^3 d\boldsymbol{r} \tag{4.8}$$

. Equation 4.7 shows that the vector matrix element is oriented to the same direction as the p-component of the excited final state orbital. Therefore, the polarization dependency of the matrix element is explained by δ, the difference of electric field $\boldsymbol{e}$ and the largest amplitude of the final state orbital $\boldsymbol{O}$, Eq. 4.5 is explained as

$$I_{if} \propto \left|\boldsymbol{e}\cdot\langle f\left|\boldsymbol{r}\right|i\rangle\right|^2 \propto \left|\boldsymbol{e}\cdot\boldsymbol{O}\right|^2 \propto \cos^2\delta \tag{4.9}$$

. For the discussion of the angular dependence of NEXAFS resonances of molecules, it is convenient to classify the molecules into groups according to the bonds, shown in Fig. 4.5. The classification consists of diatomic molecules containing single, double, and

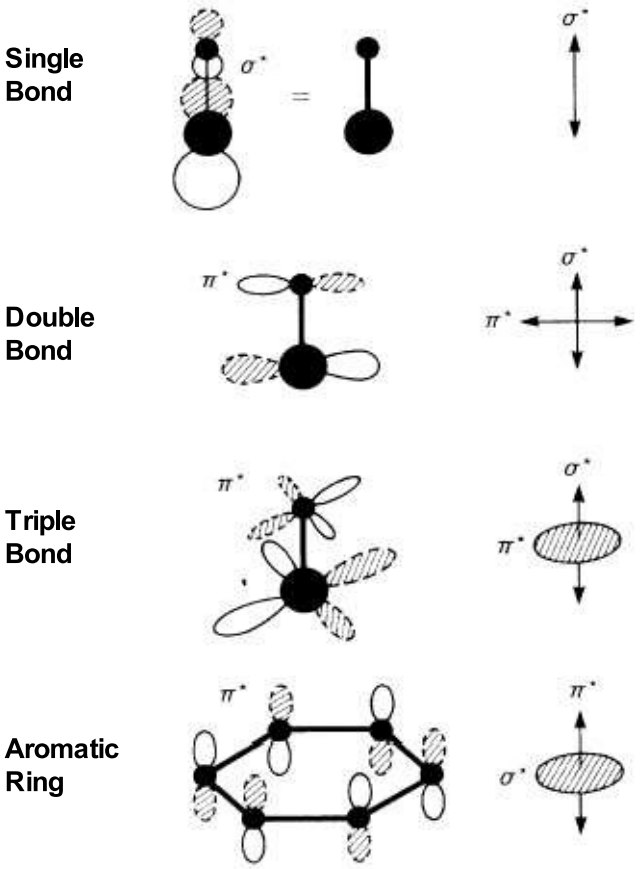

Figure 4.5: Schematic illustration of orientation of σ^* and π^* orbitals in four important groups of molecules [46].

triple bonds and a benzene ring. The orientation of σ^* and π^* orbitals of the molecules are illustrated in the figure.

In this study, the angular dependence of resonance intensity in the phosphonic acid molecules with alkyl chain was measured. The alkyl chains consists of single bonds, in which the the σ^* orbital is represented by the vector parallel to the bond.

For the polarized synchrotron light in NEXAFS measurement, the electric field vector $\boldsymbol{e}$ has two components, a component parallel to the orbit plane of the storage ring, $\boldsymbol{E}^{\parallel}$, and a component perpendicular, $\boldsymbol{E}^{\perp}$. The degree of linear polarization or the polarization factor P is expressed by

$$P = \frac{\left|\boldsymbol{E}^{\parallel}\right|^2}{\left|\boldsymbol{E}^{\parallel}\right|^2 + \left|\boldsymbol{E}^{\perp}\right|^2} \tag{4.10}$$

. Using the polarization factor P, Eq. 4.5 can be written as

$$I_{if} \propto P\left|\left\langle f\left|\boldsymbol{e}^{\parallel}\cdot\boldsymbol{p}\right|i\right\rangle\right|^2 + (1-P)\left|\left\langle f\left|\boldsymbol{e}^{\perp}\cdot\boldsymbol{p}\right|i\right\rangle\right|^2 \tag{4.11}$$

where $\boldsymbol{e}^{\parallel}$ and $\boldsymbol{e}^{\perp}$ are unit vector of the in-plane and perpendicular electric field components, respectively. The total intensity can be rewritten with the contribution of the

resonance intensity associated with $\boldsymbol{E}^{\parallel}$ components, $I^{\parallel}$, and the resonance intensity associated with $\boldsymbol{E}^{\perp}$ components, $I^{\perp}$, as

$$I \propto \left[PI^{\parallel} + (1-P)\, I^{\perp}\right] \tag{4.12}$$

. The intensity $I^{\parallel}$ and $I^{\perp}$ can be derived from the coordinate system in Fig. 4.6.

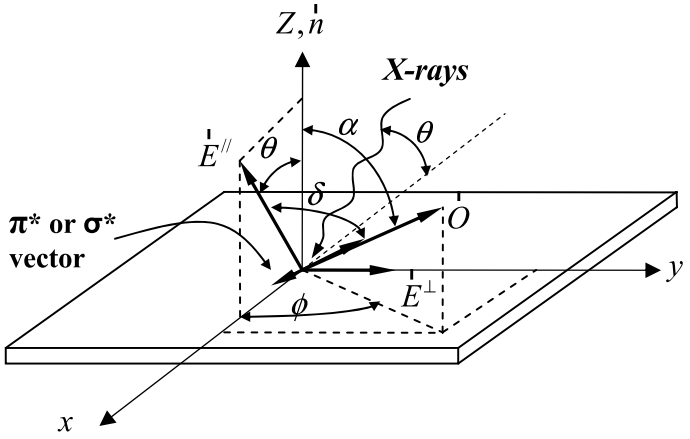

Figure 4.6: Coordinate system defining the geometry of a σ^* or π^* vector orbital on the surface [46].

As shown in Fig. 4.6, the TDM, $\boldsymbol{O}$ is characterized by a polar angle α and an azimuthal angle ϕ. The X-rays are incident in the (x, z) plane with an angle θ respect to the surface plane. Two electric field $\boldsymbol{E}^{\parallel}$ and $\boldsymbol{E}^{\perp}$ are contained in X-rays. $\boldsymbol{E}^{\perp}$ lies in the surface plane, along the y-axis. For a $1s$ initial state and a π^* or σ^* vector final state orbital, the matrix element points in the direction of the TDM, $\boldsymbol{O}$ and the intensity can be derived to be Eq. 4.9. From Eq. 4.9, the angular dependence of the resonance intensity associated with the $\boldsymbol{E}^{\parallel}$ and $\boldsymbol{E}^{\perp}$ component as

$$I^{\parallel} = A(\cos^2\theta\cos^2\alpha + \sin^2\theta\sin^2\alpha\cos^2\phi + 2\sin\alpha\cos\alpha\sin\theta\cos\theta\cos\phi) \tag{4.13a}$$

$$I^{\perp} = A(\sin^2\alpha\sin^2\phi) \tag{4.13b}$$

.

4.3.3 Dichroic Ratio [48]

Measurement of the molecule orientation function by NEXAFS intensities has an advantage that it is simply defined and without knowledge of the actual distribution function. In practice, however, only uniaxial orientation functions is deter mind. Since in some cases the surface of a sample is not a uniaxial system, it is more appropriate to use a dichroic ratio to describe the preferential alignment. The alignment in the $x-y$ surface plane is described by the dichroic ratio R_{xy}.

$$R_{xy} = \frac{I_x^{\parallel} - I_y^{\perp}}{I_x^{\parallel} + I_y^{\perp}} = \frac{I_x - I_y}{(I_x + I_y)(2P-1)} = \cos^2\phi - \sin^2\phi \tag{4.14}$$

where I_x and I_y are the measured intensity in the x and y geometries at an incidence angle of 90°, using X-rays with a degree P of linear polarization. R_{xy} is sensitive only to the in-plane orientation of final state orbital $\boldsymbol{O}$, and thus it provides a useful criterion for the degree of alignment. The R_{xy} value can theoretically vary from 1 to -1. More positive values indicate the molecular orientation normal to the substrate. $R_{xy} = 0$ represents a net balance of different orientations, in other words completely random arrangements.

4.3.4 Instrument [46]

Figure 4.7 shows a typical experimental arrangement for electron yield NEXAFS measurement. The X-ray beam from the monochrometer is first collimated by as set of movable bladesand then falls onto a metal grid with a transmission around 80%. The signal from this grid, amplified by a channeltron or spiraltron electron multiplier, serves as a dynamic reference monitor of the X-ray intensity. The grid can be coated *in situ* by evaporation of a suitable metal which does not have any absorption edges in the energy region of interest. For NEXAFS measurement, a tunable, monochromatic light source with smooth characteristics in the energy region of interest, high energy density and resolution is essential. Therefore synchrotron radiation sources are suited.

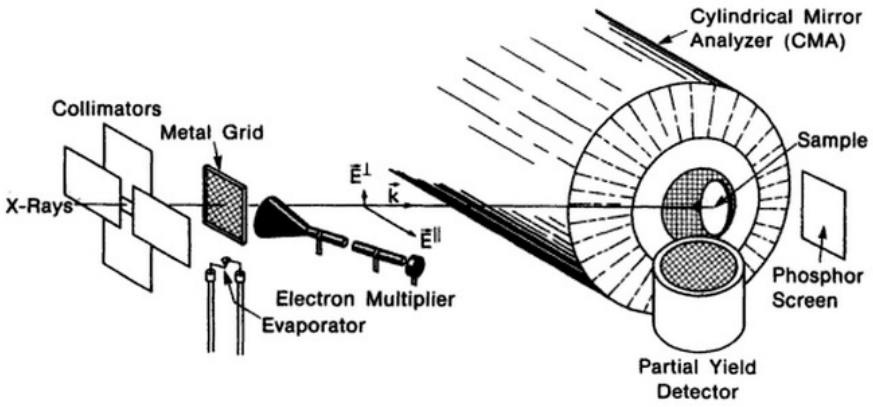

Figure 4.7: Experimental arrangement for electron yield NEXAFS measurement. The elliptically polarized X-ray beam from the monochrometer, with the major electric field vector component $E^{\parallel}$ in the horizontal plane, is collimated and then transverses as *in situ* coatable metal grid which, in conjunction with an electron multiplier, serves as a dynamic reference monitor. Electrons from the sample are detected either by an electron energy analyzer such as the shown cylindrical mirror analyzer (CMA) or a partial electron detector. A phosphor coated screen in the beam path serves for alignment purposes. [46]

Chapter 5

Optimization of Stamping Process

5.1 Procedure of Experiments

In this chapter, the effects of parameters in the stamping process to the transistor parameters were investigated Concentration of the SAMs in isopropanol solution, the stamping duration, the rinse treatment, and the anneal treatment were changed. Beside stamped SAMs, SAMs by dipping were prepared. To form SAMs by dipping, the samples were immersed into the isopropanol solution of SAM for more than 13 hours to confirm dense monolayer.

5.1.1 Electric Characteristics Measurement

Organic TFTs with the geometry shown in Fig. 3.1 were prepared in the method described in Chap. 3. Beside transistors with SAMs prepared by stamping with various parameters, transistors with SAMs prepared by dipping and without SAM were fabricated.

SAM Solution Concentration & Rinsing Effect

To investigate the effect of SAM solution concentration, sample 14P, 14Q, 14R, 14S, 14T, 14U, 14V, 15H, 15I, and 15J were fabricated.

In sample 14P, 14Q, 14R, 14S, 14T, and 14U SAMs were prepared by stamping, while in 14V, 15H, and 15I SAMs were prepared by dipping, and 15J had no SAM. In the fabrication of sample 14P, 14S, and 14V, the concentration of the isopropanol solution of HC14-PA was 1.0 mmol/ℓ; in 14Q, 14T, and 15H, 2.5 mmol/ℓ; in 14R, 14U, and 15I, 5.0 mmol/ℓ. Sample 14P, 14Q, and 14R were treated by rinsing after SAM transfer. The summary of SAM formation processes are shown in Table. 5.1.

Stamping Duration & Rinsing Effect

Effects of stamping duration, the duration of that a stamp is placed on a substrate, were investigated with sample 13A, 13B, 13C, 13D, 13E, 13F, 15A, 15B, 15C, 15D, and 15E.

Table 5.1: Summary of SAM formation conditions of the samples for anneal effect investigation.

Sample	SAM	Process	Concentration (mmol/ℓ)	Duration	Rinse	Anneal
14P	HC14-PA	Stamping	1.0	10 min	Yes	Yes
14Q	HC14-PA	Stamping	2.5	10 min	Yes	Yes
14R	HC14-PA	Stamping	5.0	10 min	Yes	Yes
14S	HC14-PA	Stamping	1.0	10 min	No	Yes
14T	HC14-PA	Stamping	2.5	10 min	No	Yes
14U	HC14-PA	Stamping	5.0	10 min	No	Yes
14V	HC14-PA	Dipping	1.0	–	Yes	Yes
15H	HC14-PA	Dipping	2.5	–	Yes	Yes
15I	HC14-PA	Dipping	5.0	–	Yes	Yes
15J			No SAM			

In the fabrication of sample 13A, reference sample, no SAM was formed; in 15A, the stamping duration was 10 s; in 13C, 30 s; in 13B and 15B, 1 min; in 13D and 15C, 5 min; in 13E and 15D, 10 min. After the formation of SAMs, sample 15A, 15B, 15C, 15D, and 15E were rinsed, while 13A, 13B, 13C, 13D, and 13E were not rinsed. The summary of SAM formation processes are shown in Table. 5.2.

Table 5.2: Summary of SAM formation conditions of the samples for stamping duration investigation, without rinse and with rinse.

Sample	SAM	Process	Concentration (mmol/ℓ)	Duration	Rinse	Anneal
13A			No SAM			
13B	HC14-PA	Stamping	1.0	1 min	No	Yes
13C	HC14-PA	Stamping	1.0	30 s	No	Yes
13D	HC14-PA	Stamping	1.0	5 min	No	Yes
13E	HC14-PA	Stamping	1.0	10 min	No	Yes
13F	HC14-PA	Dipping	1.0	–	Yes	Yes
15A	HC14-PA	Stamping	1.0	10 s	Yes	Yes
15B	HC14-PA	Stamping	1.0	1 min	Yes	Yes
15C	HC14-PA	Stamping	1.0	5 min	Yes	Yes
15D	HC14-PA	Stamping	1.0	10 min	Yes	Yes
15E	HC14-PA	Dipping	1.0	–	Yes	Yes

Annealing Effect

To investigate the effect of annealing, sample 14A, 14B, 14C, 14D were fabricated.

In sample 14A and 14B, HC14-PA SAMs were formed by stamping, while in sample 14C and 14D SAMs were formed by dipping. Sample 14A and 14C were annealed at 100°C for 10 minutes. All samples were rinsed with pure isopropanol before annealing. The SAM formation methods and treatments are summarized in Table. 5.3.

Table 5.3: Summary of SAM formation conditions of the samples for SAM concentration effect investigation.

Sample	SAM	Process	Concentration (mmol/ℓ)	Duration	Rinse	Anneal
14A	HC14-PA	Stamping	1.0	10 min	Yes	Yes
14B	HC14-PA	Stamping	1.0	10 min	Yes	No
14C	HC14-PA	Dipping	1.0	–	Yes	Yes
14D	HC14-PA	Dipping	1.0	–	Yes	No
14E			No SAM			

Distribution

To investigate the uniformness in the devices characteristics prepared by stamping, 20×25 transistors were fabricated either by stamping or dipping. In sample 17, HC14-PA SAM was formed by dipping. In sample 18, HC14-PA SAM was formed by stamping, then rinsed and annealed. An optical image of the stamping process on the device is shown in Fig. 5.1(a) and completed device is shown in Fig. 5.1(b). The formation process is summarized in Table. 5.4. Among the transistors, 130 transistors were measured.

Table 5.4: Summary of preparation conditions of the samples for distribution measurement.

Sample	SAM	Process	Concentration (mmol/ℓ)	Duration	Rinse	Anneal
17	HC14-PA	Dipping	1.0	–	Yes	Yes
18	HC14-PA	Stamping	1.0	10 min	Yes	Yes

5.1.2 SAM Analysis

Contact Angle

Contact angles of 1 $\mu\ell$ water droplets on Al/AlO_x/SAM structures were measured to determine the existence of SAMs on AlO_x substrates.

On Si/SiO_2 substrate, 40-nm-thick Al layer was deposited. The surface was oxidised with plasma. SAMs were transferred by either dipping or stamping on sample. On sample 12B, HC14-PA was formed by dipping; on 12C, HC14-PA was stamped then rinsed; on 12D, HC14-PA was stamped; on 12E, FC8-PA was formed by dipping; on 12F, FC8-PA

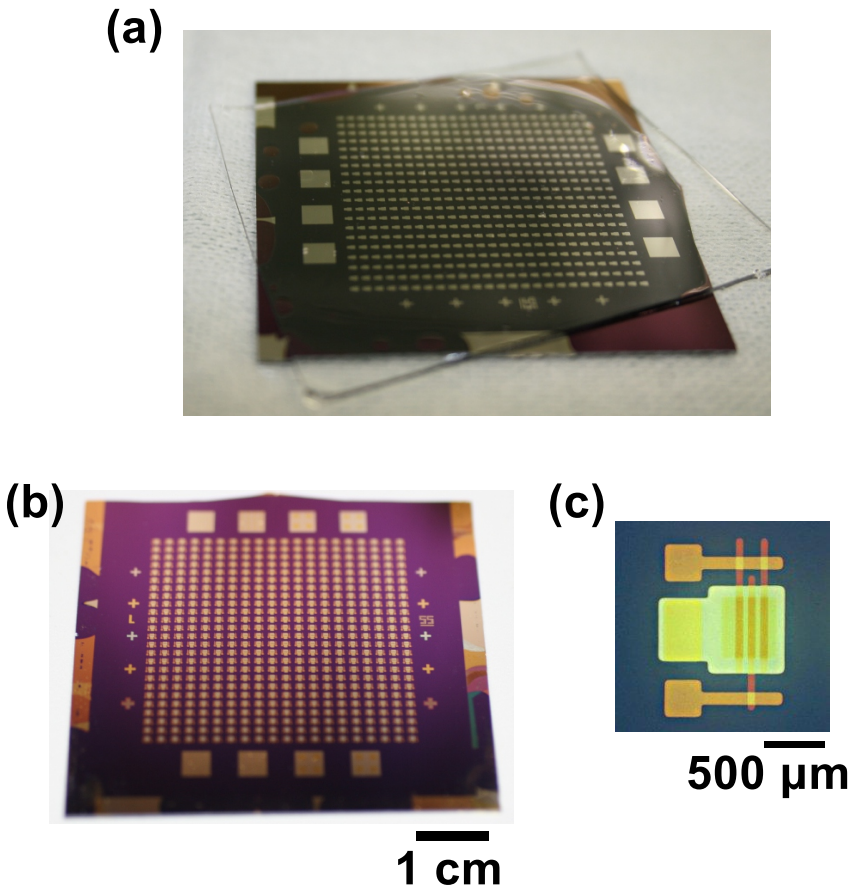

Figure 5.1: Optical images of fabrication and completed 20×25 transistors; (a) stamping process, (b) completed device, and (c) single transistor, with W/L = 1000/50.

was stamped by stamping then rinsed; on 12G, FC8-PA was stamped. The preparation methods are summarized in Table. 5.5.

Table 5.5: Summary of SAM formation conditions of the samples for TEM observation.

Sample	SAM	Process	Concentration (mmol/ℓ)	Duration	Rinse	Anneal
12A			No SAM			
12B	HC14-PA	Dipping	1.0	–	Yes	Yes
12C	HC14-PA	Stamping	1.0	10 min	Yes	Yes
12D	HC14-PA	Stamping	1.0	10 min	No	Yes
12E	FC8-PA	Dipping	1.0	–	Yes	Yes
12F	FC8-PA	Stamping	1.0	10 min	Yes	Yes
12G	FC8-PA	Stamping	1.0	10 min	No	Yes

TEM Observation

The cross-sections of Al/AlO_x/SAM/Au capacitor structures of sample 7R, 7S, and 7U and Al/AlO_x/Au reference sample 7P were imaged by transmission electron microscopy (HF-9000UHE TEM, 300 kV, Hitachi High-Tech Manufacturing & Service Corporation). On sample 7P, no SAM was formed; on 7R, HC14-PA SAM was formed by stamping then annealed; on 7S, HC14-PA SAM was formed by stamping then rinsed and annealed; on 7U, HC14-PA SAM was formed by dipping. After the formation of dielectrics, Au top electrodes were deposited on all samples. The SAM formation methods and treatments are summarized in Table. 5.6.

Table 5.6: Summary of SAM formation conditions of the samples for TEM observation.

Sample	SAM	Process	Concentration (mmol/ℓ)	Duration	Rinse	Anneal
7P			No SAM			
7R	HC14-PA	Stamping	1.0	10 min	No	Yes
7S	HC14-PA	Stamping	1.0	10 min	Yes	Yes
7U	HC14-PA	Dipping	1.0	–	Yes	Yes

NEXAFS Measurement

Samples for NEXAFS measurement and organic TFTs for process optimization were prepared. For the samples for the NEXAFS measurement, sample 13NA, 13NB, 13NC, 13ND, and 13NE with the geometry of Al/AlO_x/HC14-PA were prepared.

In sample 13NA, HC14-PA was stamped on plasma-activated AlO_x for 10 minutes, then rinsed with pure isopropanol and annealed at 100°C for 10 minutes; in sample

13NB, HC14-PA was stamped for 10 minutes, then rinsed; in sample 13NC, HC14-PA was stamped for 10 minutes on AlO_x, without rinsing and annealing; in sample 13ND, HC14-PA was stamped for 1 minute, then rinsed and annealed; in sample 13NE, HC14-PA SAM was formed by dipping, then rinsed and annealed. The preparation conditions are summarized in Table. 5.7.

Table 5.7: Summary of preparation conditions of the samples for NEXAFS measurement.

Sample	SAM	Process	Concentration (mmol/ℓ)	Duration	Rinse	Anneal
13NA	HC14-PA	Stamping	1.0	10 min	Yes	Yes
13NB	HC14-PA	Stamping	1.0	10 min	Yes	No
13NC	HC14-PA	Stamping	1.0	10 min	No	No
13ND	HC14-PA	Stamping	1.0	1 min	Yes	Yes
13NE	HC14-PA	Dipping	1.0	–	Yes	Yes

5.2 Results

5.2.1 Electric Characteristics Measurement

SAM Concentration & Rinse Effect

The capacitances in SAM capacitors prepared with SAM solutions of different concentrations are shown in Fig. 5.2(a) and Thicknesses calculated from the capacitance assuming the permittance of HC14-PA SAM as 2.5 [49] are shown in Fig. 5.2(b). The capacitances of all the devices with SAMs were in the range expected from previous reports: close to 800 nF/cm^2 [50]. Clear trends that the capacitance decrease as the solution concentration increases in stamped samples and the capacitance increase as the solution concentration increases in dipped samples are observed. Comparing the rinsed and non-rinsed samples, the rinsed samples always showed larger capacitance and smaller thickness. All samples with SAM showed smaller capacitance value.

Threshold voltages, mobilities, and on/off ratios of transistors in the SAM concentration and rinse effect investigation are shown in Fig. 5.3. As for the mobility, the similar trends as the capacitance are observed in the Fig. 5.3(a): The mobility increases as the SAM concentration increases in dipped samples, while the mobility decreases as the SAM concentration decreases in stamped samples. The threshold voltages in both stamped and rinsed samples and dipped samples prepared with the solution thicker than 2.5 mmol/ℓwere almost equivalent. As for the on/off ratio, higher concentration solution resulted in larger value.

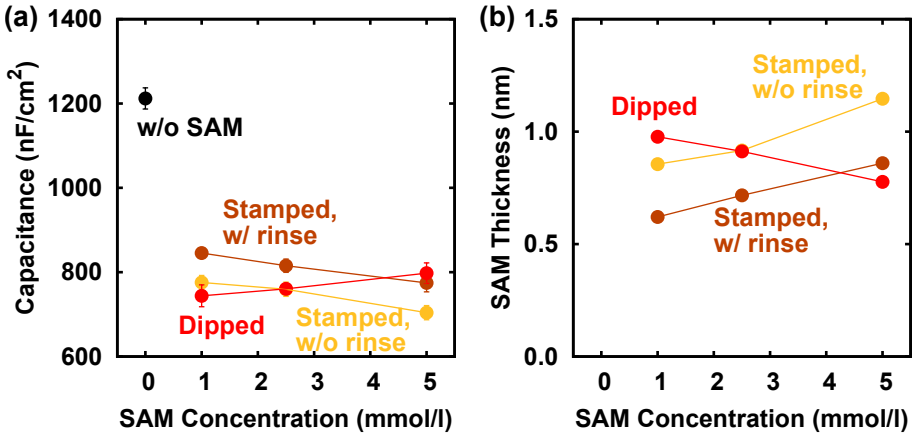

Figure 5.2: (a) Capacitance of SAM capacitors and (b) thickness of SAMs calculated from the capacitance in the SAM concentration effect investigation as functions of solution concentration. The plotted points are colored according to the SAM formation process.

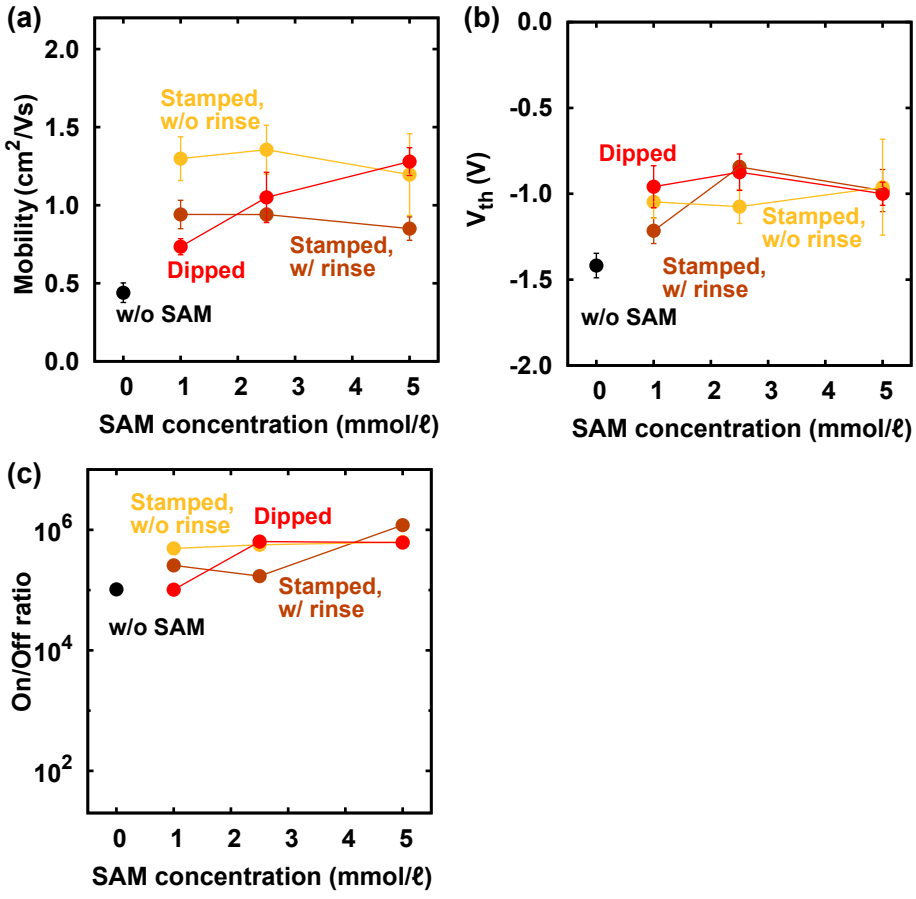

Figure 5.3: Transistor parameters in the solution concentration effect investigation; (a) mobility, (b) threshold voltage, and (c) on/off ratio as functions of solution concentration. The plotted points are colored according to the SAM formation process.

Stamping Duration & Rinse Effect

The capacitances in SAM capacitors prepared with SAM solutions with different concentrations are shown in Fig. 5.4(a) and thicknesses calculated from the capacitance are shown in Fig. 5.4(b). With low concentration of the solution less than 1 mmol/ℓ, the difference in the capacitance was small, about 35 nF/cm^2 by 1 min stamping, while the difference increased to 125 nF/cm^2 by longer stamping. Also, comparing the 5 min stamping and 10 min stamping, the capacitance by 10 min stamping was slightly smaller in both of rinsed and non-rinsed samples. The stamped samples always had smaller capacitance than dipped sample.

Threshold voltages, mobilities, and on/off ratios of transistors in the SAM concentration and rinse effect investigation are shown in Fig. 5.5. The DNTT semiconductor layers in rinsed samples and non-rinsed samples were not deposited at the same time, and the DNTT quality widely varies depending on the deposition condition. Therefore it is not appropriate to compare the parameter values in rinsed samples and non-rinsed samples, However, in both of rinsed samples and non-rinsed samples, it is observed that the smallest mobility was obtained by shortest stamping duration, 30 s for non-rinsed samples and 15 s for rinsed samples, as shown in Fig. 5.5(a). By 1 min stamping, the mobility increased drastically. As for the threshold voltage, no clear trends were observed. On/off ratio in the rinsed samples by 1 min stamping was relatively small value, which might be due to the error in the operation during the fabrication, since other samples showed rather uniform values. Excluding this point, the on/off ratio in the shortest stamping duration was smallest in both of rinsed and non-rinsed samples.

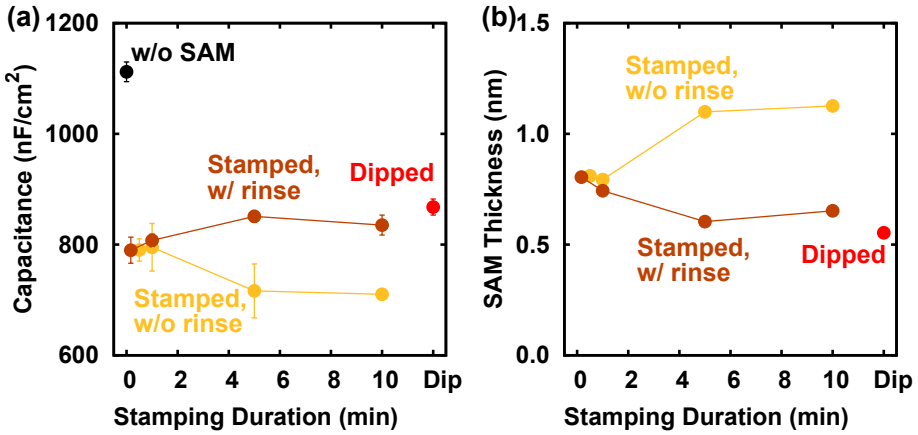

Figure 5.4: (a) Capacitance of SAM capacitors and (b) thickness of SAMs calculated from the capacitance in the stamping duration effect investigation as functions of stamping duration. The plotted points are colored according to the SAM formation process.

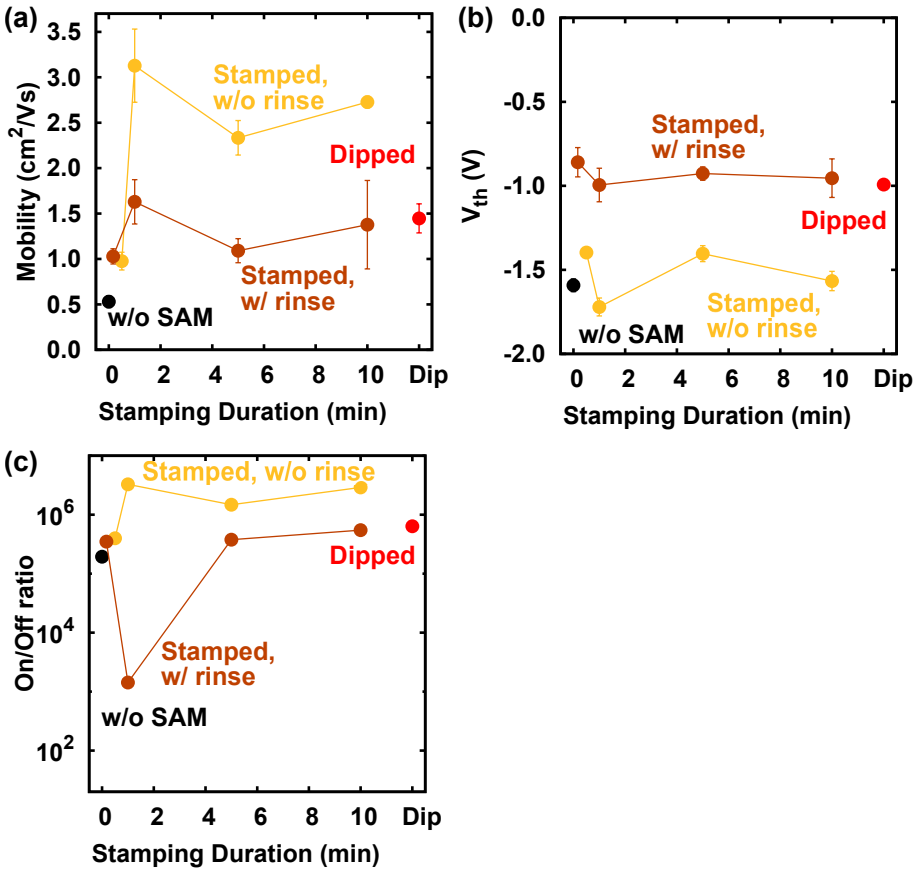

Figure 5.5: Transistor parameters in the stamping duration effect investigation; (a) mobility, (b) threshold voltage, and (c) on/off ratio as functions of the stamping duration. The plotted points are colored according to the SAM formation process.

Annealing Effect

The capacitances in SAM capacitors prepared with and without annealing are shown in Fig. 5.6(a) and thicknesses calculated from the capacitance are shown in Fig. 5.6(b). Sample 14A showed smallest capacitance and largest SAM thickness, while other samples with SAM showed almost equivalent values.

Threshold voltages, mobilities, and on/off ratios are shown in Fig. 5.7. By annealing, the overall parameter decreased in the stamped samples, while in the dipped samples the overall parameters increased. The differences in threshold voltage and on/off ratio in either formation process, either treatment were almost negligible.

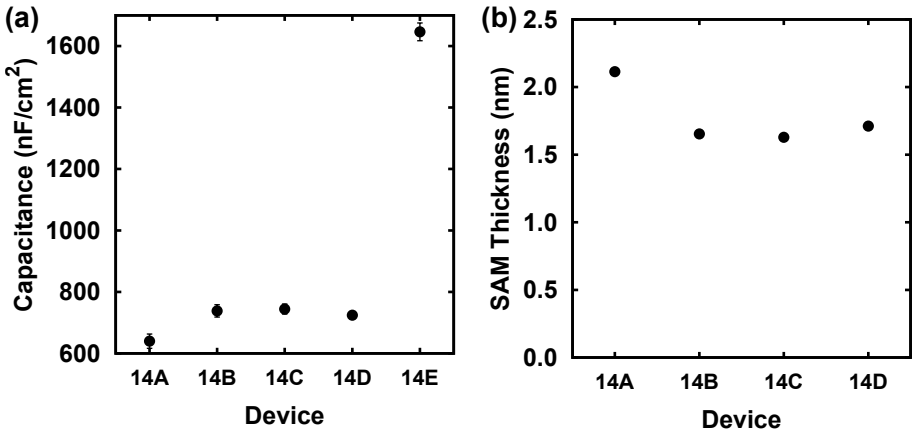

Figure 5.6: (a) Capacitance of SAM capacitors and (b) thickness of SAMs calculated from the capacitance in the annealing effect investigation.

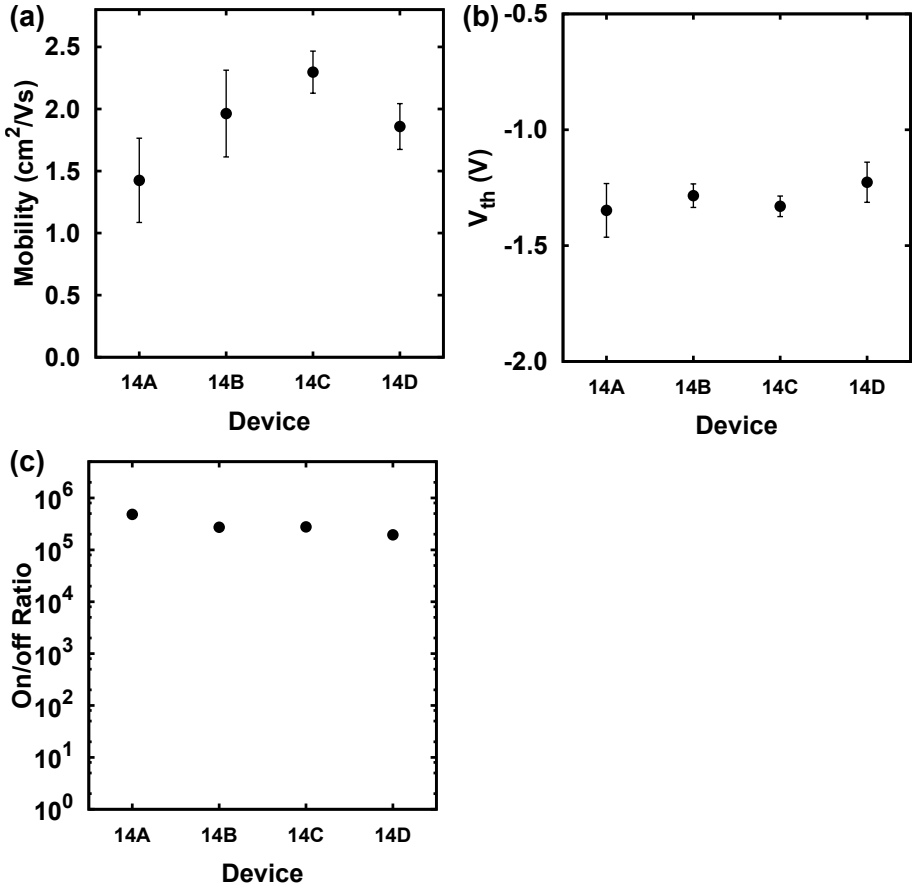

Figure 5.7: Transistor parameters in the annealing effect investigation; (a) mobility, (b) threshold voltage, and (c) on/off ratio.

Distribution

Among the 130 transistors measured in both sample 17 and 18, 115 transistors and 117 transistors had no obvious damage nor disconnection and showed transistor characteristics, respectively. Then yield was calculated under a rule that a transistor which has leakage current larger than 10^{-7} A at V_{DS} = -3 V is defined as a "failed device". Under the rule, the yield of stamped SAM (sample 18) and dipped SAM (sample 17) was 117/128 and 115/117, respectively. According to the geometry, distributions of leakage current, threshold voltage, mobility, and on/off ratio were mapped. The result is shown in Fig. 5.8.

Here, on/off ratio can be a criterion for yield calculation, however, small on/off ratio around 10^2–10^3 was observed in many transistors as shown in Fig. 5.8(g) and (h). This may be caused by the loose contact of the metal shadow mask to the substrate during the deposition of source and drain electrodes. Also, on/off ratio can be affected by the local condition of the semiconductor. On the other hand, the quality of gate dielectric is most dominant factor to affect leakage current. Therefore, to evaluate the distribution of only SAM layer, leakage current was adopted as a criterion.

From the mappings in Fig. 5.8, it can be seen that the stamped sample had somewhat larger distribution than dipped sample, especially the abrupt change of mobility at the middle of the sample.

The histograms of mobility, threshold voltage, and on/off ratio is shown in Fig. 5.9. The average value and standard deviation is summarized in Table. 5.8. As can be seen in Fig. 5.8, larger distribution in stamped device was observed.

Table 5.8: Statistics of transistor characteristics in sample 17 and 18.

Sample	Process	Mobility (cm^2/V·s)	Threshold Voltage (V)	On/off Ratio
17	Dipping	1.37 ± 0.50	-1.01 ± 0.13	9.82 $\times 10^4$
18	Stamping	1.80 ± 0.88	-1.21 ± 0.32	9.07 $\times 10^5$

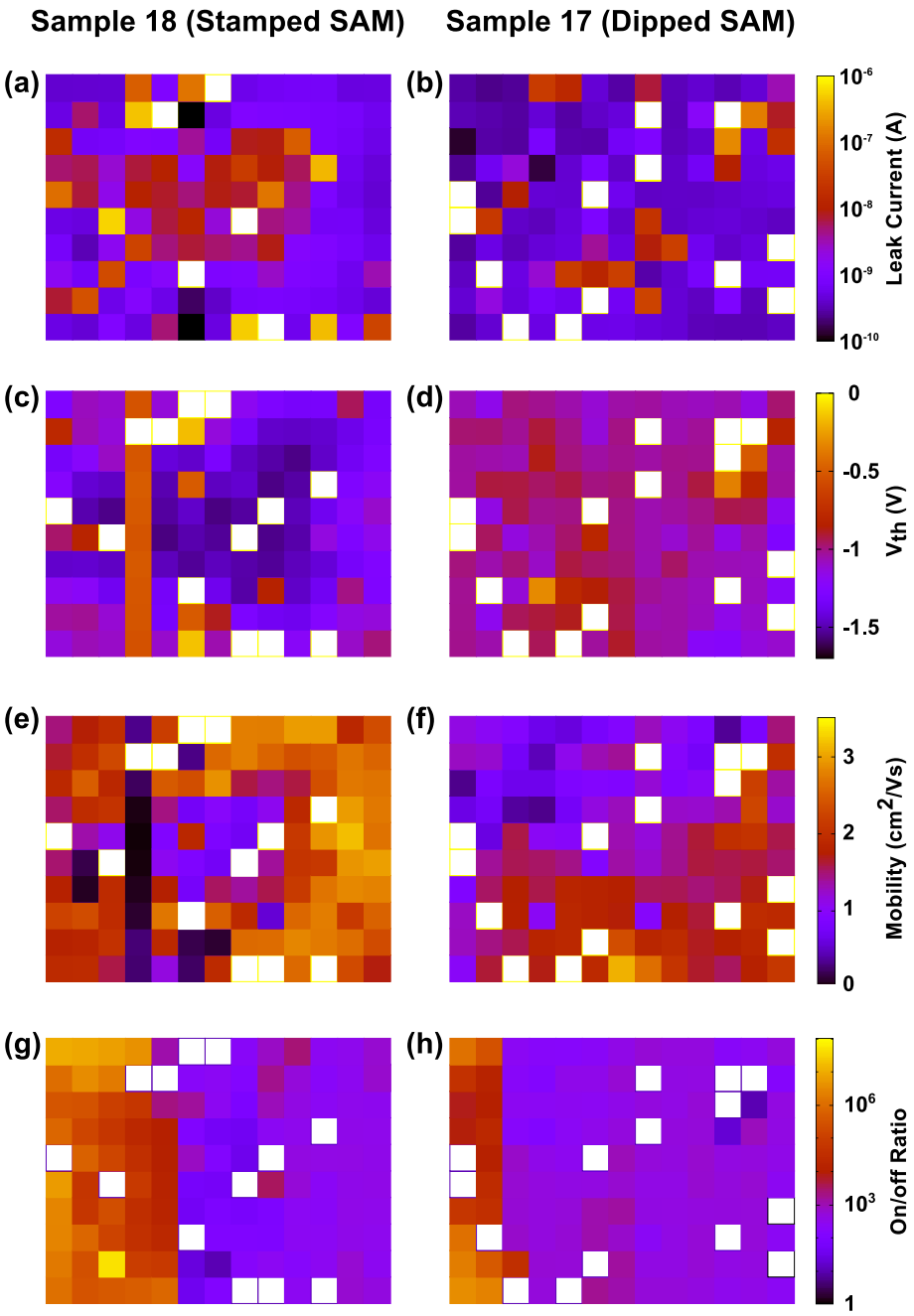

Figure 5.8: Characteristics of transistor in 20 × 25 sample. Failed devices are colored in white. (a) Leakage current distribution of sample 18 at V_{GS}= -3 V, (b) that of sample 17, (c) threshold voltage distribution of sample 18, (d) that of sample 17, (e) mobility distribution of sample 18, (f) that of sample 17, (g) on/off ratio distribution of sample 18, (h) that of sample 17.

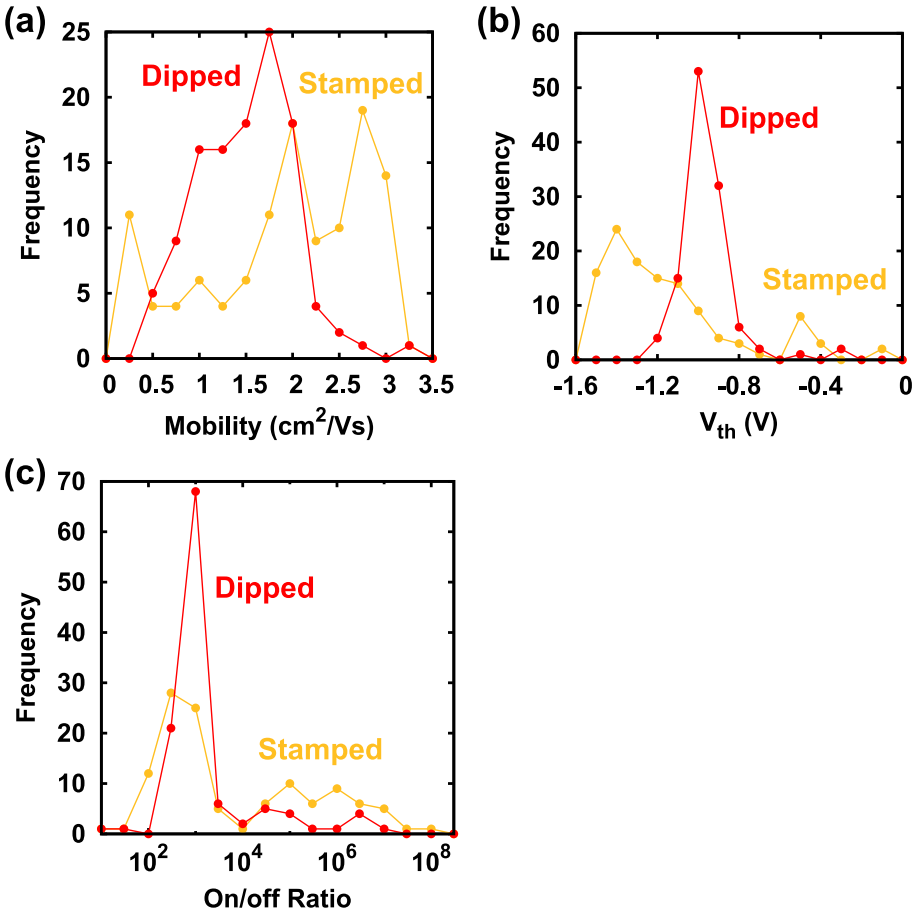

Figure 5.9: Histograms of transistor characteristics in sample 17 (dipped) and 18 (stamped); (a) mobility, (b) threshold voltage, and (c) on/off ratio.

5.2.2 SAM Characterization

Contact Angle

The results of contact angle measurements are shown in Fig. 5.10 and contact angle measurements are shown in Fig. 5.11. The contact angles of water droplets on SAMs, either dipped or stamped, were 99–105° and significantly larger than the contact angle of water droplet on AlO_x, 71°.

Since the surface of $AlO_x$is very hydrophobic and the surface of phosphonic acids assembled on AlO_x is very hydrophioic, the large contact angles of SAMs formed on AlO_x indicates the existence of the molecules on AlO_x by dipping or stamping.

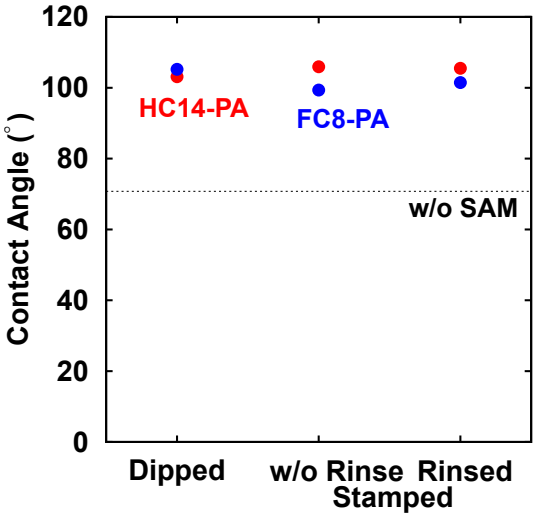

Figure 5.10: Contact angles of SAMs formed on plasma-activated AlO_x layer by each method.

TEM Observation

The capacitance of the sample 7P, 7R, 7S, 7U are shown in Fig. 5.12(a). The capacitance decrease by forming SAMs is clearly observed. By treating the formed SAM by rinsing, the slight increase in the capacitance and the decrease in the thickness is observed as in Fig. 5.12(b), which is consistent with the results above. Compared with treatments, the dipped SAMs had largest capacitance.

High-resolution cross-sectional images of TEM observation of the samples are shown in Fig. 5.13. The thin SAM layer is clearly resolved in the transmission electron micrograph, *i.e.* the formation of SAM layer is confirmed in stamped samples and dipped sample. The thickness of the SAMs are 1 nm or less than 1 nm, which are coincident with the thickness calculated from the capacitance measurement in Fig. 5.12(b). From the thickness and Fig. 5.13, it can be concluded that by either stamping or dipping, only one monolayer is formed.

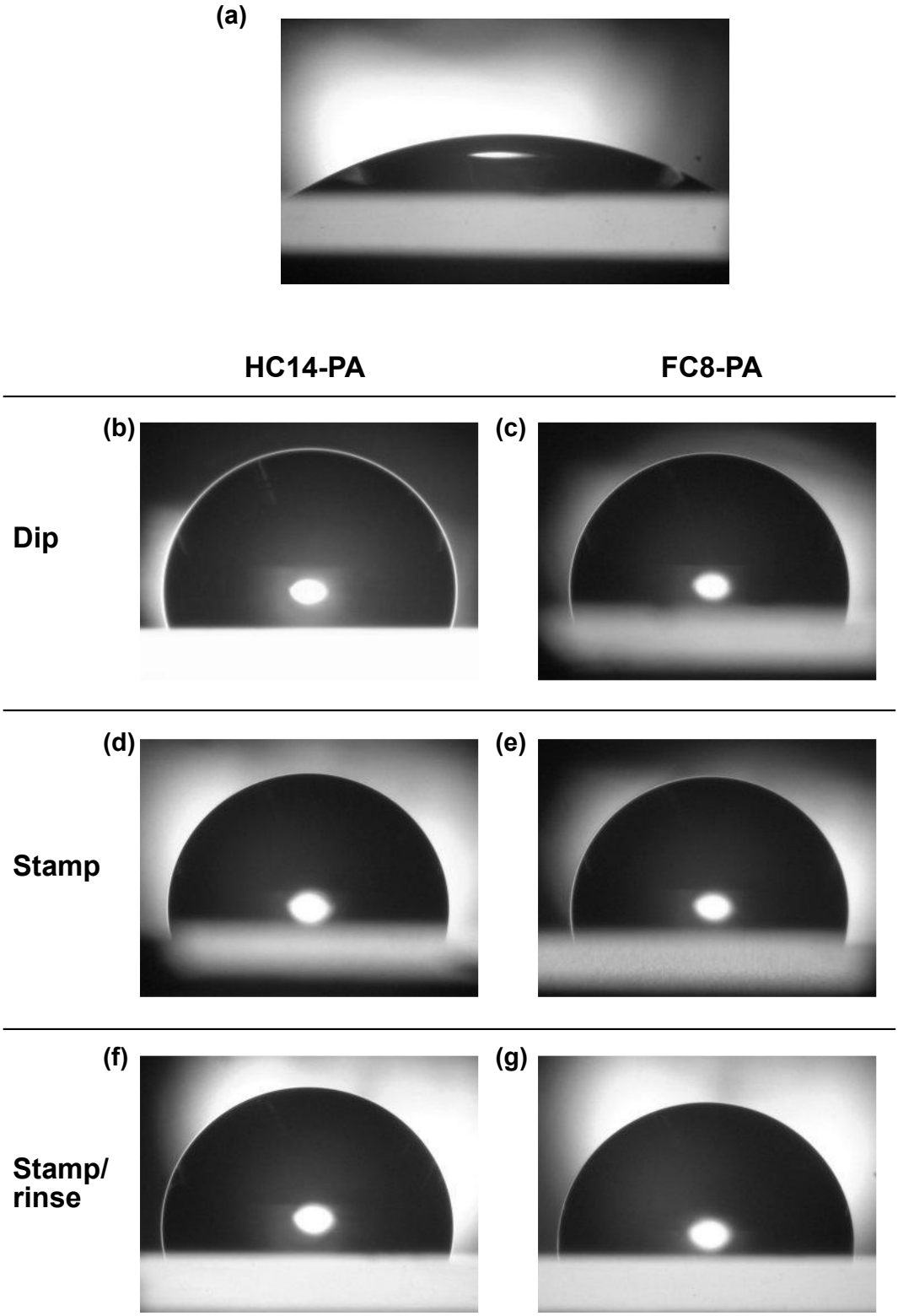

Figure 5.11: Water contact angles measured on SAMs. (a) 12A, (b) 12B, (c) 12E, (d) 12D, (e) 12G, (f) 12C, (g) 12F.

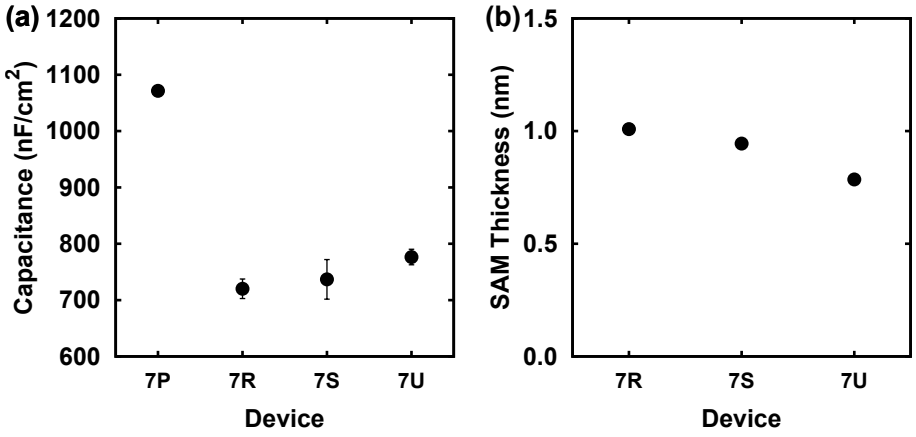

Figure 5.12: (a) Capacitance of SAM capacitors and (b) thickness of SAMs calculated from the capacitance in the SAM capacitors with different treatments.

NEXAFS Measurement

The SAMs formed by stamping and conventional dipping were analyzed by NEXAFS measurement to specify the structure of the monolayers. The results are shown in Fig. 5.14 and Fig. 5.15.

NEXAFS PEY spectra or HC-14PA SAMs prepared by different methods for different incident angles are shown in Fig. 5.15(a-e). The intensity peaks were at 293 eV corresponding to C–C σ^* resonance with $\theta = 75°$ and at 288.5 eV corresponding to C–H* resonance with $\theta = 35°$. In all samples, the clear shift of the peaks from 293 eV to 288.5 eV can be seen as the incident angle θ increases. This shift of the peak indicates that the molecules are aligned almost normal to the AlO_x surface, since the TDM $\boldsymbol{O}$ of C–C bond is parallel to the direction of C–C bond itself and the absorb intensity is explained by Equation 4.9. From these results, it can be concluded that the SAM molecules self-assembled normal to the AlO_x with head groups down to the substrate, as like dipped SAMs, by stamping.

Figure 5.15(a) shows the dichroic ratio of each sample at the incident angle of 55°. The difference in each treatment is small, though sample 13NB and 13ND show smaller dichroic ratios, while sample 13NA, 13NC, 13NE show larger dichroic ratios. From the result, it can be concluded that the SAMs were transferred uniaxially to some degree, not randomly. This conclusion is quite consistent with the result of contact angle measurement.

Figure 5.15(b) shows the tilt angles of each sample. Tilt angle determines the thickness of the SAM and the molecule density. Therefore smaller tilt angle indicates larger molecule density. From the result, it can be concluded that annealing and longer stamping have an effect to increase the tilt angle.

Figure 5.15(c) shows the PEY spectra of the intensity at the incident degree $\theta = 55°$ and (d) shows the intensity of absorption at post edge 318 eV. The absorption intensity directly indicates the coverage of the substrate surface. In this measurement, non-rinsed sample 13NC shows the largest intensity, which is explained as the excess molecules were

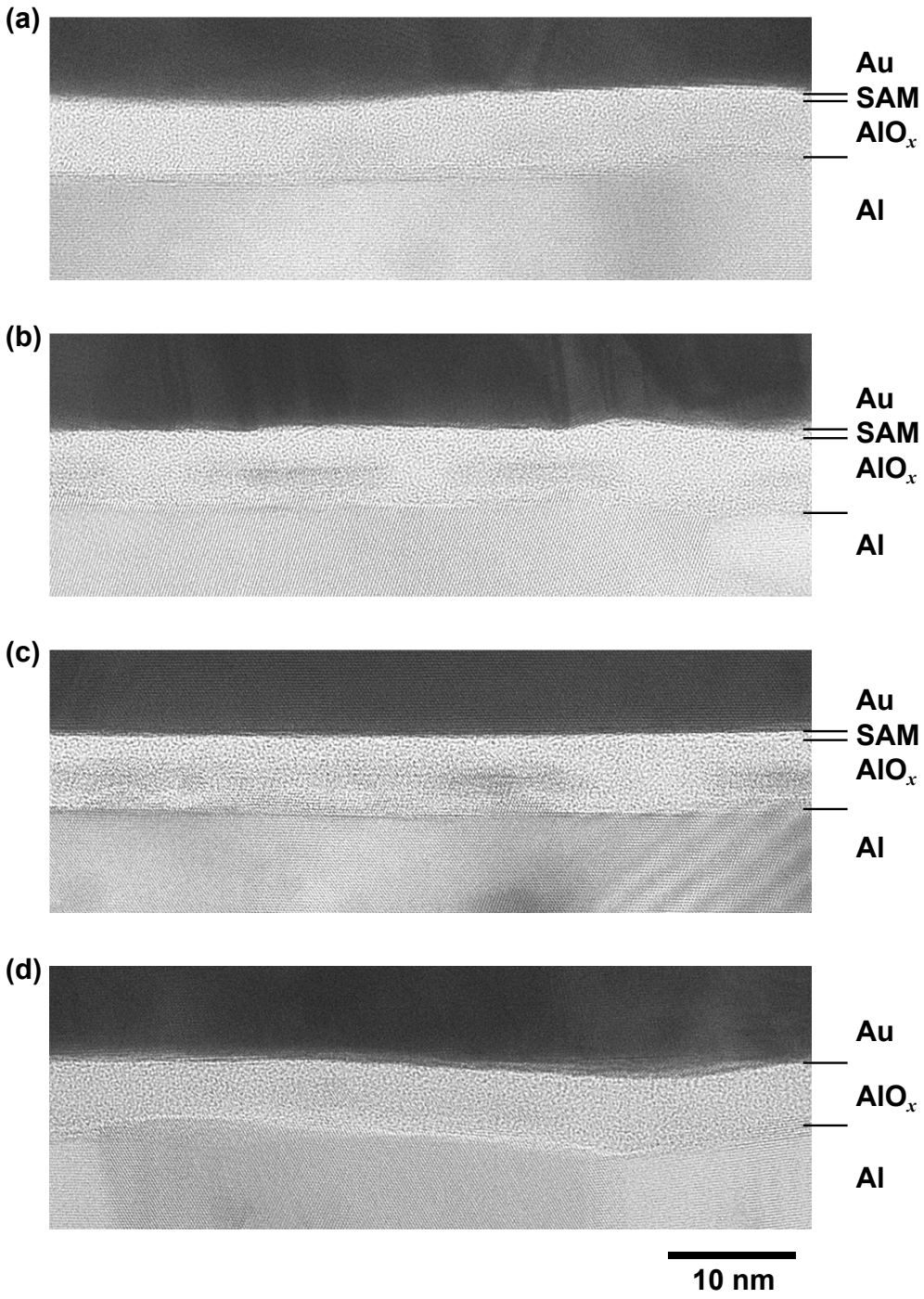

Figure 5.13: Cross-sectional TEM images of Al/AlO_x/SAM/Au capacitor structures and Al/AlO_x/Au reference sample, imaged using H-9000UHE TEM under V_{acc} of 300 kV, by Hitachi High-Tech Manufacturing & Service Corporation. The SAM in each sample was formed and treated in different methods. (a) Sample 7R; the SAM was formed by stamping, then annealed at 100°C for 10 min. (b) Sample 7S; the SAM was formed by stamping, then rinsed with pure isopropanol and annealed at 100°C for 10 min. (c) Sample 7U; the SAM was formed by dipping, then rinsed with pure isopropanol and annealed at 100°C for 10 min. (d) Sample 7P; reference sample, without SAM.

washed away by rinsing. Sample 13NA and 13NC, in which SAMs were formed by 10-min stamping, showed almost equivalent value to sample 13NE, in which SAM was formed by dipping. Sample 13ND, in which SAM was formed by 1 min stamping, showed the smallest intensity, indicating the smallest coverage.

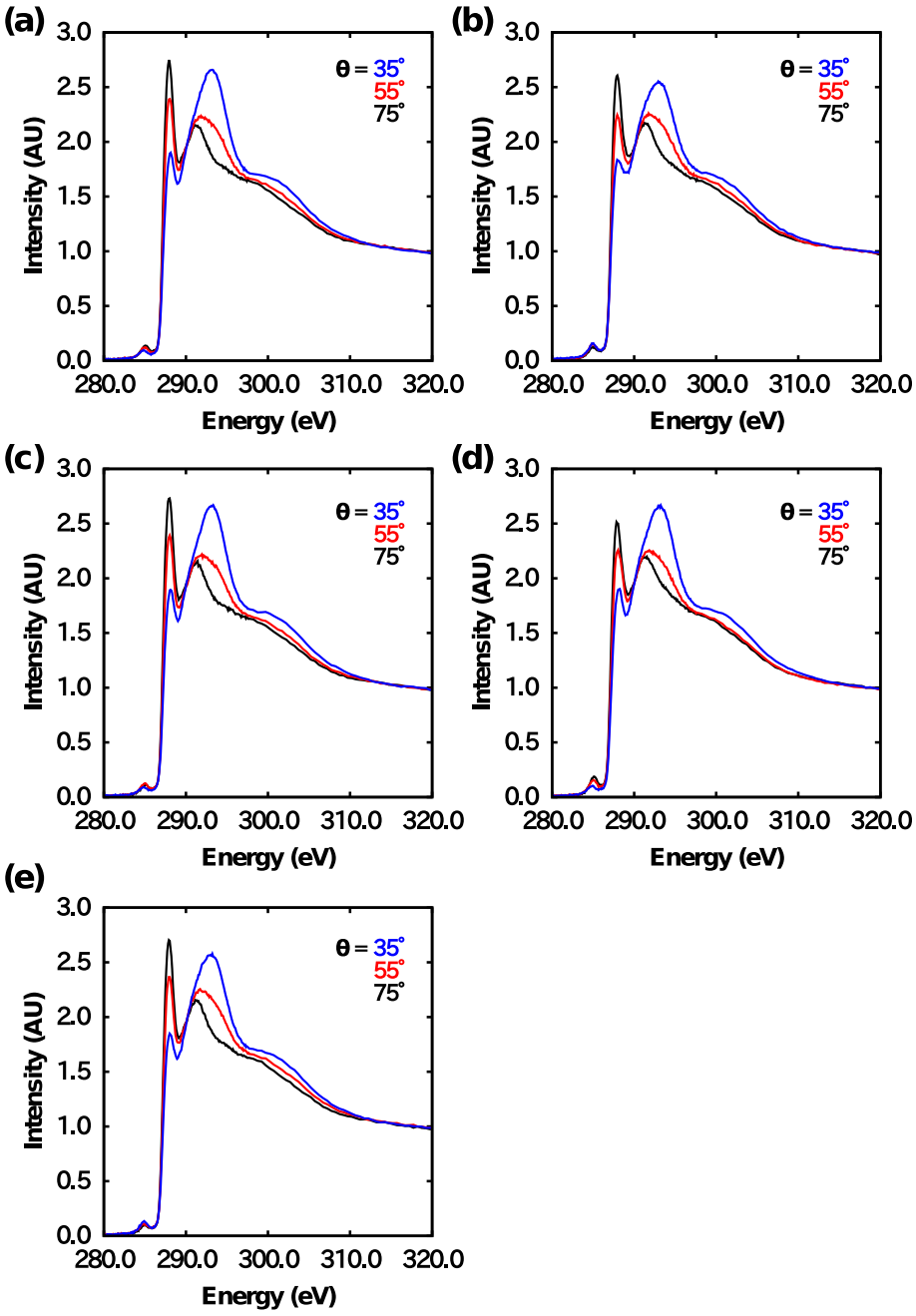

Figure 5.14: NEXAFS PEY spectra for HC14-PA prepared by different methods for different incident angles. (a) Sample 13NA; (b) sample 13NB; (c) sample 13NC; (d) sample 13ND; (d) sample 13NE.

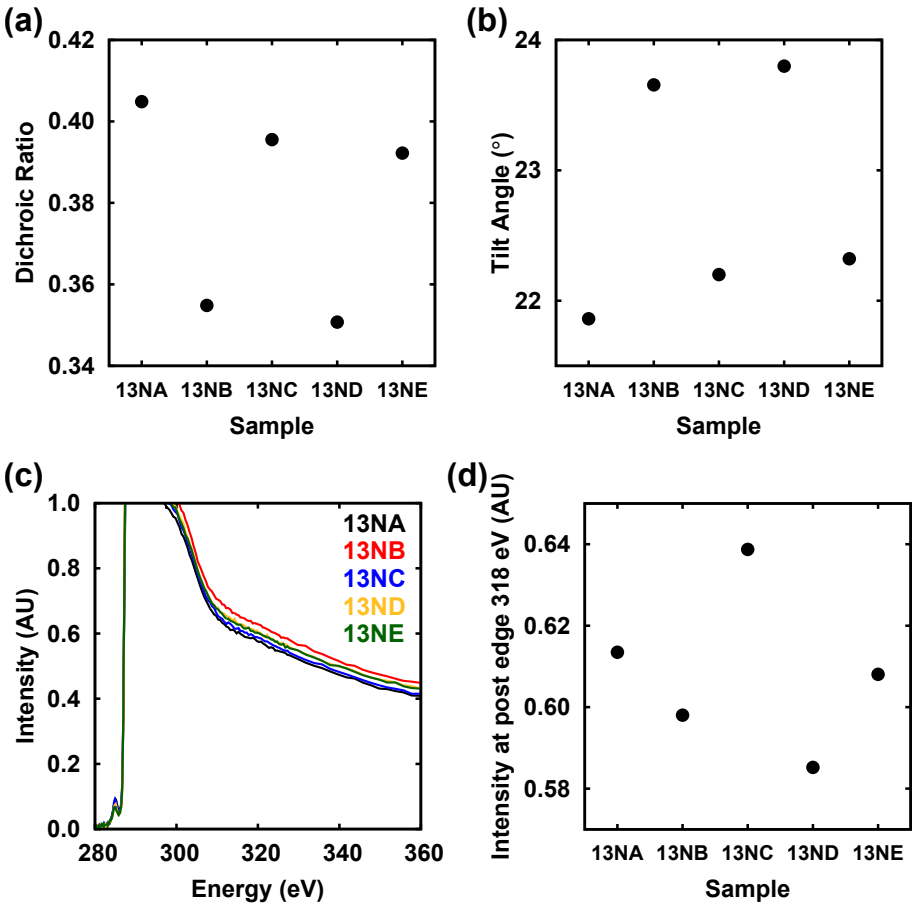

Figure 5.15: Parameters extracted from NEXAFS PEY measurement. (a) Dichroic ratio of each sample. (b) Tilt angles of HC14-PA molecules on AlO_x in each sample. (c) Comparison PEY spectra of the intensity of each sample. (d) Intensity of each sample at post edge 318 eV.

5.3 Discussion

The main interest in the SAM analysis is the alignment of the molecules in SAMs formed by stamping. In the dipping process, the SAM molecules have enough free space in the solution. By the chemical reaction and the intermolecular force, the molecules assemble spontaneously and in order, with the head group to the substrate. However, in the stamping process, the direction and the orientation of the molecules on the stamp were not known. Also due to the less freedom between the stamp and the substrate, the final state of the molecules after transferred onto the substrate was questioned and not investigated before. Therefore it was critical problem whether the "self-assembled monolayer" was formed by stamping like by dipping.

In this work, the formation and the fine structures of SAMs formed by stamping were investigated by various measurements. First, by contact angle measurement, the SAM transfer was confirmed. The large contact angles on SAM layer indicates hydrophilic head groups contacted to the substrate and hydrophobic groups appeared to the surface. Next, the cross-section of the SAM capacitor was observed by TEM in Fig. 5.13. The thickness calculated from the capacitance and the thickness observed from the TEM image, about 1 nm, were coincident. Also, from the cross-section images, the formation of single layer was confirmed. Finally, by NEXAFS measurement, details of the SAM structure were investigated in Fig. 5.14 and 5.15. Most importantly, the alignment of the SAM molecules were confirmed to be aligned as like the SAMs formed by dipping, with head groups connected to the AlO_x surface.

With the results above, it can be said that the SAM molecules transferred onto the PDMS stamp is *not* strongly bonded to the PDMS stamp surface. Therefore, when the PDMS stamp is placed onto the activated AlO_x surface, the strong bond of the chemical resonance between the AlO_x and phosphonic acid group surpasses the weak bond between the SAM molecules and the PDMS surface, and the SAM molecules aligns as like the self-assemble in the liquid.

The second interest is the excess or deficiency of the molecules. In the top-contact, bottom-gate geometry which is applied in this work, the smooth interface between the gate dielectrics and semiconductor is considered to be critical to obtain higher mobility. The excess of the molecule decreases the interface quality, while the deficiency of the molecules causes the pinholes in the gate dielectrics and high off- and leakage current. The quality of SAM can be described by both the capacitance and the transistor parameters. Especially the value of the capacitance can be a good material assessment, since the transistor parameters depends on the evaporation of the semiconductor and contact electrodes as well as the gate dielectrics. In the dipping process, the amount of the molecules adsorbed on the AlO_x surface is spontaneously optimized since the molecules have freedom in liquid and therefore the dipping process is considered to be robust. In the stamping process, however, the process parameters such as the solution concentration, stamping duration, rinse, and anneal directly affect the amount of the molecules adsorbed on the

AlO_x substrate.

The effect of the solution concentration was small for the stamping process but larger for the dipping process. In the stamping process, the capacitance decreased as the concentration increased and opposite effect was observed in the dipping process as observed in Fig. 5.2(a). Assuming that all SAM had same permittance, the result indicates that by higher solution concentration, the more molecules were adsorbed to the substrate by stamping, This is because the amount of the molecules that reacts with the AlO_x substrate simply depends on the solution concentration. Also, it can be thought that there was always the excess of the molecules by stamping rather than deficiency. In the stamped samples, the mobility decreased as the concentration increased (Fig. 5.3(a)). Assuming that the genuine difference between the samples with different solution concentration is only the surface of the gate dielectrics, the decrease in the mobility can be caused by the excess molecules. Moreover, the on/off ratio of the stamped samples were always larger than the sample without SAM (Fig. 5.3)(c), which indicates that the SAM layers had low density of pinholes to reduce off-current.

The stamping duration had large effect to the capacitance and transistor parameters. As for the stamping duration, the trends of the changes of the capacitance in Fig. 5.4 and mobility in Fig. 5.5 show that the threshold duration of the adsorption is around 1 min, which is consistent with the previous study [51]. By stamping shorter than 1 min, the values change drastically while the values are mostly saturated by the longer stamping. Though SAM can be formed in a few tens of seconds [52], to obtain adequately dense and smooth layer, stamping more than 1 min is required. To confirm high quality SAMs, longer stamping is effective. However, 5 min stamping is long enough in the aspects of capacitance, mobility, threshold voltage, and on/off ratio.

Rinsing had effects to increase the capacitance significantly and to decrease the distribution of the capacitance, however, rinsing decreases the mobility and on/off ratio. As explained above, the excess molecules are removed by rinsing. In Fig. 5.4(a) and (b), this removal effect is clearly observed in the stamping longer than 1 min.

Annealing has little effect to the value of the capacitance, however, the improvement in the mobility was observed.

In large-size fabrication, the average values of transistor characteristics were better in stamped device. However, more uniform characteristics was obtained in dipped device.

In the stamping process, non-uniformity is inevitable. The characteristics in each single device strongly depends on the gate dielectrics. During the stamping process, parameters such as the concentration gradient on the stamp, pressure applied on the stamp, and so on, can always cause non-uniformity in SAM. In addition, the distribution increases as the fabrication size increases. In small devices, such as 20-transistor device shown in Fig. 3.1(c), distribution in the transistor characteristics is largely suppressed due to the size; for example, in Fig. 5.3, the distribution in the characteristics in stamped devices were almost equivalent to that of dipped devices. On the other hand, as it can be seen in Fig. 5.9, large distribution in stamped device was clearly observed. However, please

note that the order of distribution value is equivalent in stamped and dipped samples. It can be said that stamping can be applied to circuits which requires preciseness of dipping.

Chapter 6

Control of Threshold Voltage

6.1 Procedure of Experiments

6.1.1 Single Transistor

Stamping Without Rinse

Two species of SAMs, HC14-PA and FC18-PA, were formed on one substrate in different region of one sample labeled as 7D and 7E. To prevent the cross contaminate of HC14-PA and FC18-PA, samples were not rinsed. As reference samples, sample 7A, 7B and 7C were prepared with dipped HC14-PA, FC18-PA, and without SAM, respectively. SAM formation conditions are summarized in Table. 6.1.

Table 6.1: Summary of SAM formation conditions of the samples for TEM observation.

Sample	SAM	Process	Concentration (mmol/ℓ)	Duration	Rinse	Anneal
7A	HC14-PA	Dipping	1.0	–	Yes	Yes
7B	HC14-PA	Dipping	1.0	–	Yes	Yes
7C			No SAM			
7D, 7E	HC14-PA, FC18-PA	Stamping	1.0	10 min	No	Yes

Stamping With An Extra Rinse Process

The effect of rinse was investigated when two species of SAMs were formed on separate regions in one substrate. was investigated. On sample 7P and 7Q, SAM of HC14-PA and FC8-PA, was stamped, respectively. On sample 7R and 7T, HC14-PA and FC8-PA were stamped in different regions on the same one sample then rinsed. On sample 7S, HC14-PA and FC8-PA were stamped in different regions. On sample 7U, no SAM was formed.

Table 6.2: Summary of SAM formation conditions of the samples for TEM observation.

Sample	SAM	Process	Concentration (mmol/ℓ)	Duration	Rinse	Anneal
9P	HC14-PA	Stamping	1.0	10 min	Yes	Yes
9Q	FC8-PA	Stamping	1.0	10 min	Yes	Yes
9R, 9T	HC14-PA, FC18-PA	Stamping	1.0	10 min	Yes	Yes
9S	HC14-PA, FC18-PA	Stamping	1.0	10 min	No	Yes
9U			No SAM			

6.1.2 Load Inverter

Two single transistors were connected to form an load inverter as shown in Fig. 6.1. The input-output characteristics and the gain were measured. In both the load transistor M_{load} and the drive transistor M_{drive}, the threshold voltages were controlled by stamping different SAMs.

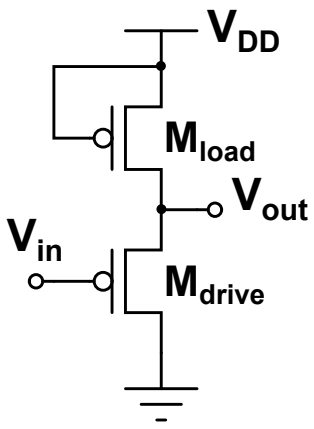

Figure 6.1: Schematics diagram of a load inverter.

6.2 Results

SAM Capacitor

Figure 6.2 shows the capacitance frequency response. It can be seen that the capacitances of all the devices with SAMs were in the range expected from previous reports: close to 800 nF/cm^2 for HC14-PA [50] and (600 ± 100) nF/cm^2 for FC18-PA [19]. Note that dipped samples always exhibit larger capacitance than stamped samples. Assuming that the dielectric constant of SAMs is 2.5 [53], the thickness of the SAM layers was evaluated from the capacitance as 0.9 and 1.2 nm for dipped and stamped HC14-PA layers, respectively, as compared to 1.4 and 2.7 nm for dipped and stamped FC18-PA layers, respectively, which were very close to the SAM molecule length of 2.3 nm.

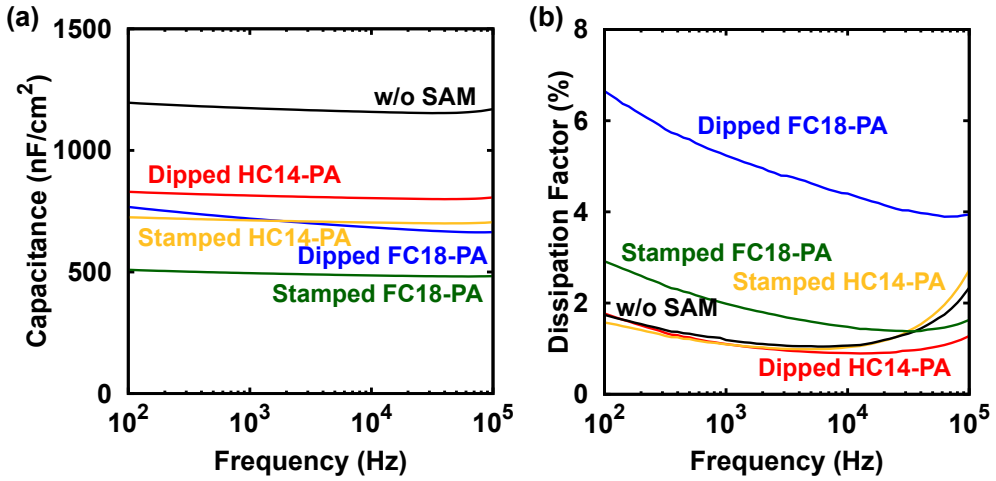

Figure 6.2: (a) Capacitance as a function of frequency under a bias voltage of 1 V, (b) Dissipation factor as a function of frequency under a bias voltage of 1 V.

Leakage Current

Figure 6.3 shows the leakage current density measured on Al/AlO_x/SAM/Au capacitors (without semiconductor) based on SAMs of either HC14-PA or FC18-PA prepared by both stamping and dipping, plus a control device without SAM. The top surface size for the Au electrodes was $700 \times 100\mu m^2$. In Fig. 6.3, it can be seen that all the capacitors with SAMs, either dipped or stamped, exhibited a current density that was two or three orders of magnitude smaller than that without SAM, confirming the important role of SAM in suppressing gate leakage. The difference in current density demonstrates that a pinhole-free thin layer was formed during the stamping process. Also note that leakage currents of the stamped SAM devices were smaller than that of dipped SAM samples, which have previously shown the ability to integrate at the circuit level [3].

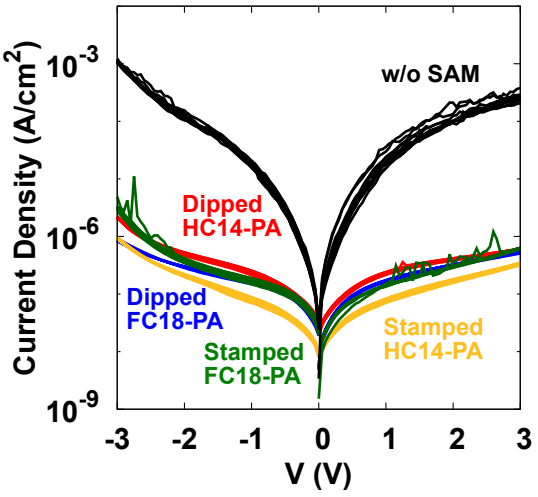

Figure 6.3: Leakage current density as a function of bias voltage measured on five different SAM capacitors. Each measurement was repeated on ten junction to evaluate uniformity.

DNTT Surface Analysis

From the morphology of the SAM layer, the uniformity and the degree of assemble is directly observed, however, the SAM surface analysis is difficult due to static electrical charge. On the other hand, the surface analysis of the semiconductor layer is relatively easy and the quality of organic semiconductors is very sensitive to the surface morphology of the underneath layer [21]. The smooth surface enables better crystal growth *i.e.* the crystal growth in larger size. Therefore, the size of the organic semiconductor crystal represents the quality of SAM layers underneath.

Figure 6.4 shows the AFM image of DNTT layer deposited on each SAM layers on AlO_x. Each sample size was 2.5×2.5 μm^2, and the grain sizes are summarized in Table 6.3. The surface morphology of DNTT grains on dipped SAM is different from that on stamped SAM, which can be ascribed to the difference of the surface smoothness of SAM layers even though the average thickness was one or two monolayers for both HC14-PA and FC18-PA samples. It is important to remember that the leakage current of stamped samples was smaller than that of dipped samples, as shown in Fig 6.3. Although this is an indirect measurement, it still provides evidence that the possible existence of sub-monolayer coverage can be excluded.

Table 6.3: Summary of DNTT grain size (nm^2) deposited on each SAM species or AlO_x.

Formation	HC14-PA SAM	FC18-PA SAM
Dip	37 195	83 127
Stamp	33 803	31 123
W/o SAM	24 414	

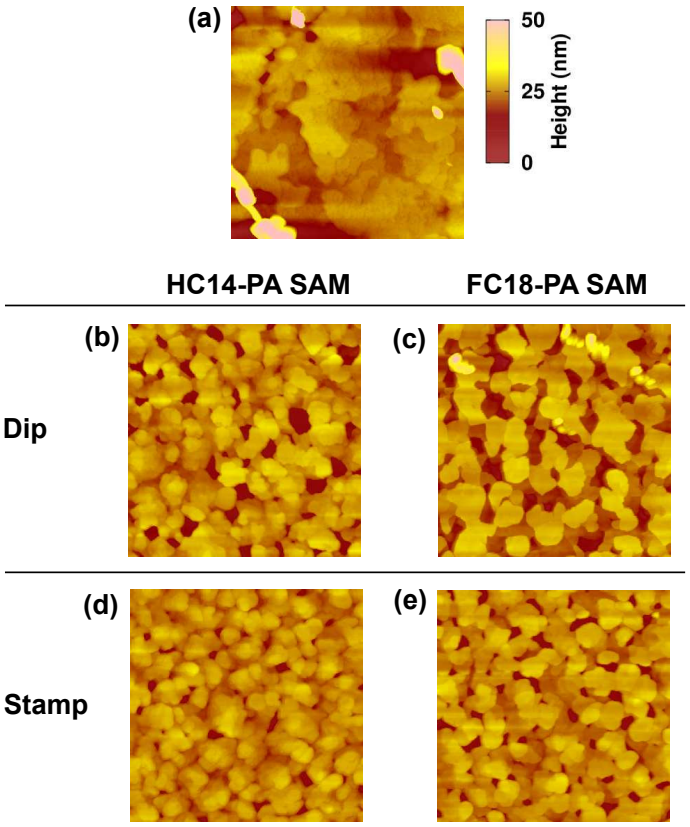

Figure 6.4: AFM images of 2.5×2.5 μm^2 squares of DNTT layers deposited on stamped or dipped SAMs or on AlO_x. For each sample, average grain size was calculated. (a) On AlO_x for reference, (b) on dipped HC14-PA SAM, (c) on dipped FC18-PA SAM, (d) on stamped HC14-PA SAM, (e) on stamped FC18-PA SAM.

6.2.1 Electric Characterization

Stamp Without Rinse

The representative transfer and output curves for transistors without SAMs and those with dipped or stamped HC14-PA SAMs are shown in Fig. 6.5(a, b) and those with dipped or stamped FC18-PA SAMs are shown in Fig. 6.5(c, d). The mobilities and the threshold voltages were extracted from the transfer curves along with the field-effect mobilities and on/off ratio. The mobility and the threshold voltage in each transistor on sample 7D and 7E are plotted according to the device geometry in Fig. 6.6. The shift of the threshold voltage in each region is clearly observed. The parameters are summarized in Fig. 6.7.

Regardless of the process and/or species of SAM, all samples with SAMs exhibited higher mobility than those without SAM, as expected [21]. The HC14-PA samples had a higher mobility than the FC18-PA samples, which is also in line with previous reports [32, 17, 18].

Furthermore, all the samples with SAMs exhibited higher on/off ratios than those samples without SAMs, as a result of smaller gate leakage currents. Most importantly,

the select of SAM molecule has a pronounced effect on the threshold voltage of the TFTs, regardless whether the SAMs were prepared by stamping or dipping, as it can be clearly seen in Fig. 2(a). The difference in threshold voltage between TFTs with HC14-PA and TFTs with FC18-PA was 0.83 V, which is about 42% of the supply voltage (2 V). Systematic changes of the threshold voltages were clearly observed, although the distribution of stamped samples was slightly larger than that of dipped samples.

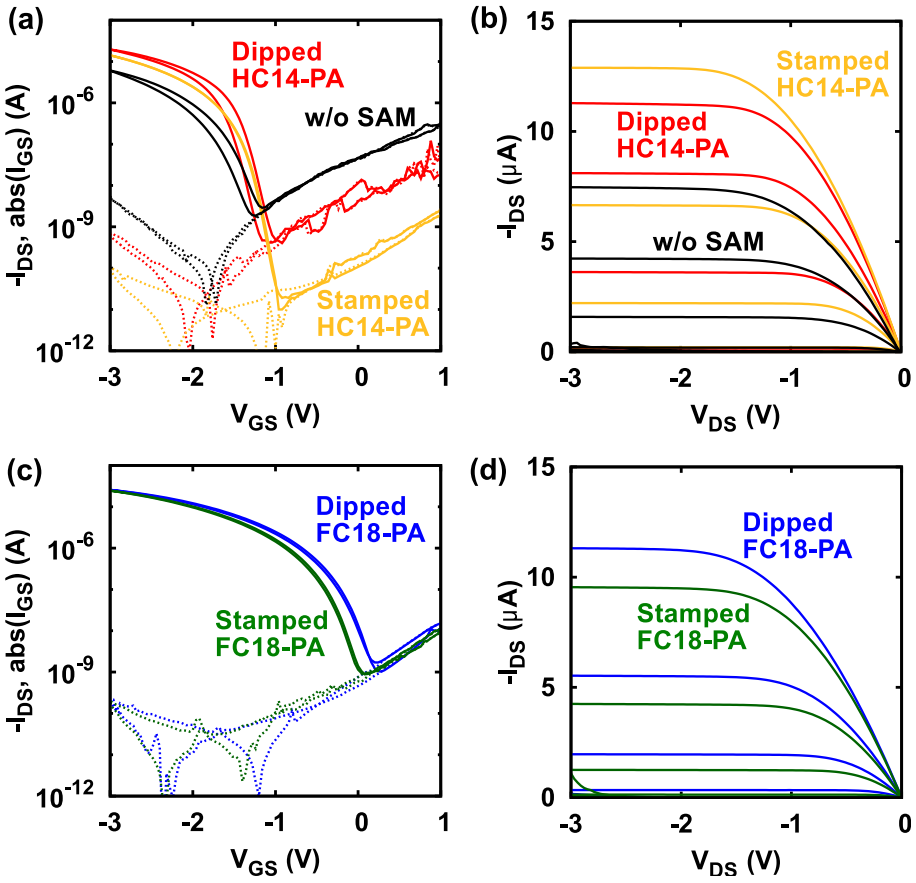

Figure 6.5: (a, b) Transfer and output characteristics of DNTT transistors with SAM of dipped HC14-PA, stamped HC14-PA, without SAMs, and (c, d) with SAM of dipped FC18-PA, stamped FC18-PA. In (a) and (c), I_{DS} is drawn with solid lines and I_{GS} is drawn with dotted lines. curves: I_{DS}, dotted curves: I_{GS}). the measurements were performed with a drain–source voltage V_{DS} = —-2 V.

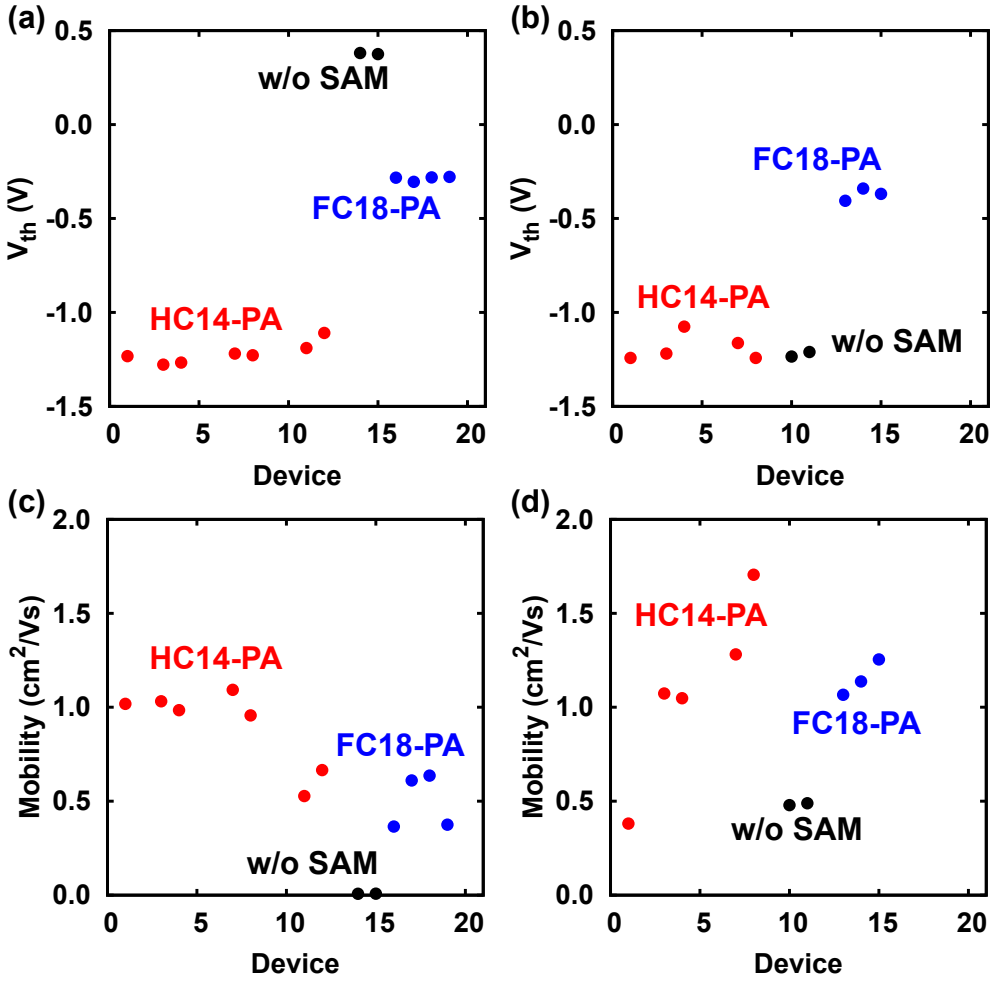

Figure 6.6: Threshold voltages and mobilities of transistors in sample 7D and 7E. (a) Threshold voltages in sample 7D. (b) Mobilities in sample 7E. (c) Threshold voltages in sample 7D. (d) Mobilities in sample 7E. SAM in each transistor is colored according to the species.

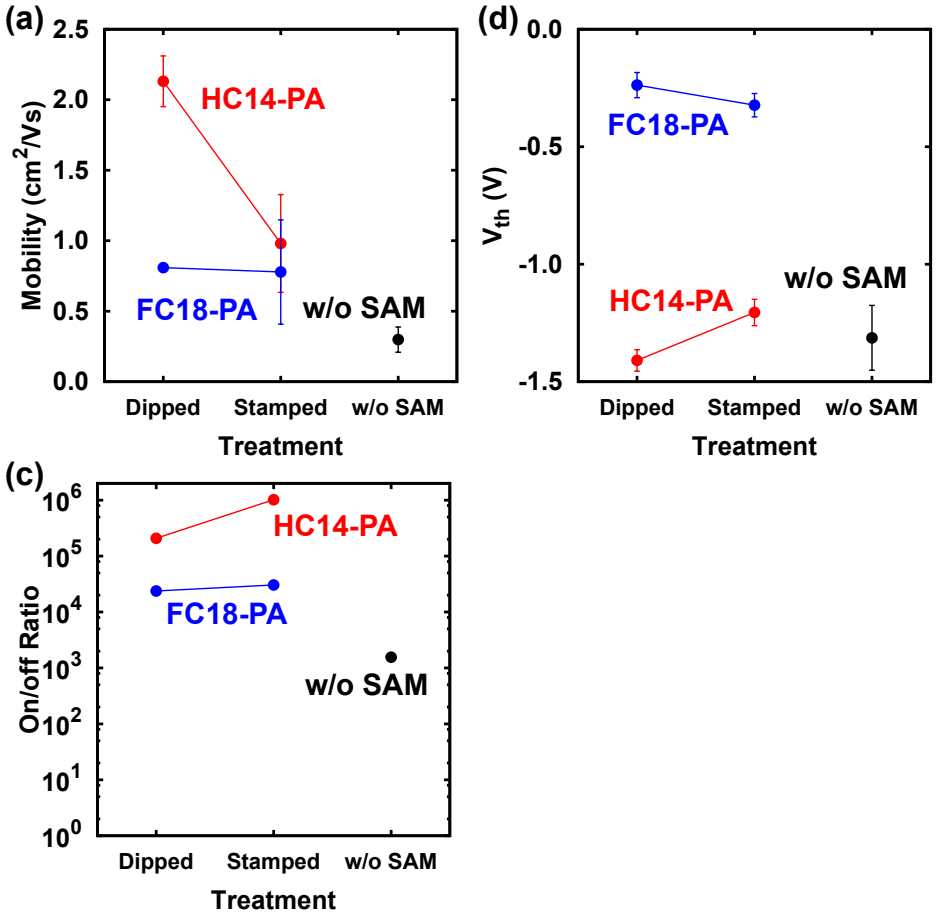

Figure 6.7: Summary of parameters in samples with dipped or stamped HC14-PA or FC18-PA, or without SAM; (a) mobility, (b) threshold voltage, (c) on/off ratio. The plotted points are colored according to the SAM species.

Stamp With An Extra Rinse Process

The representative transfer and output curves for transistors without SAMs and those with dipped or stamped HC14-PA SAMs are shown in Fig. 6.8(a, b) and those with dipped or stamped FC8-PA SAMs are shown in Fig. 6.8(c, d). From the transfer and output characteristics, no large difference by caused rinse is observed.

Mobility and threshold voltage are plotted according to the geometry in Fig. 6.9. Comparing HC14-PA-stamped region and FC8-PA-stamped region, neither the shift in the threshold voltage nor the increase in the mobility were observed.

The parameters in each sample are summarized in Fig. 6.10. The averaged values also show no significant change caused by rinse, but the distribution of value was decreased by rinse process.

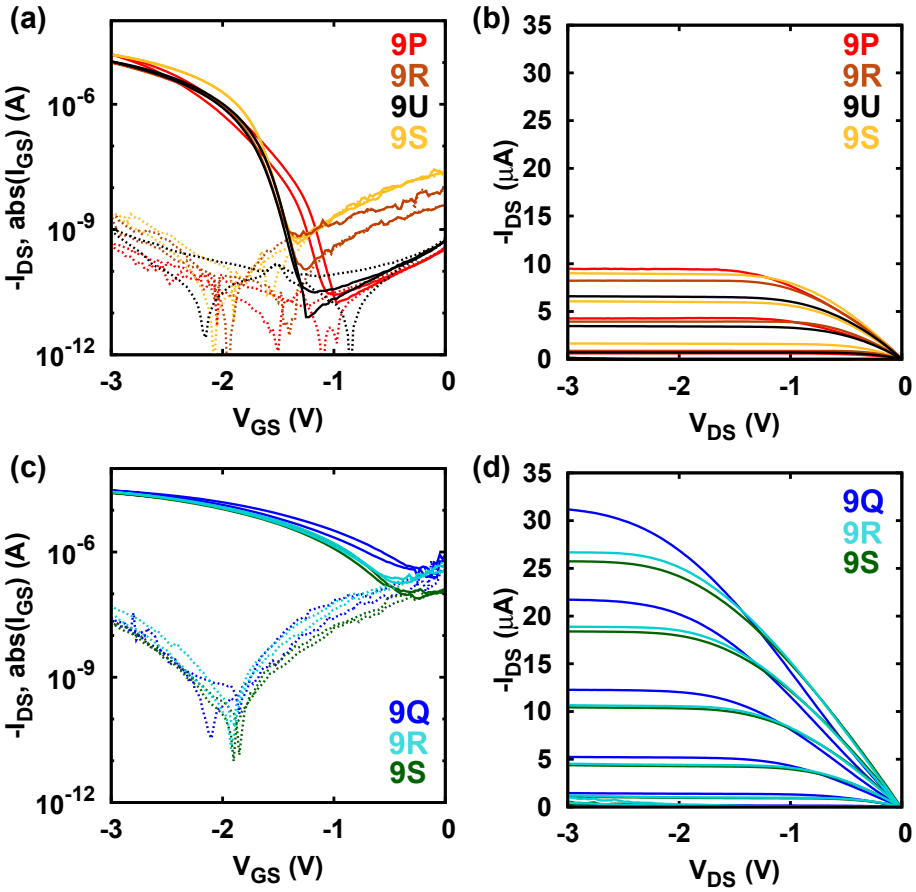

Figure 6.8: (a, b) Transfer and output characteristics of DNTT transistors with stamped HC14-PA and without SAM. (c, d) Transfer and output characteristics of DNTT transistors with stamped FC8-PA. In (a) and (c), I_{DS} is drawn with solid lines and I_{GS} is drawn with dotted lines. curves: I_{DS}, dotted curves: I_{GS}). the measurements were performed with a drain–source voltage V_{DS} = —-2 V.

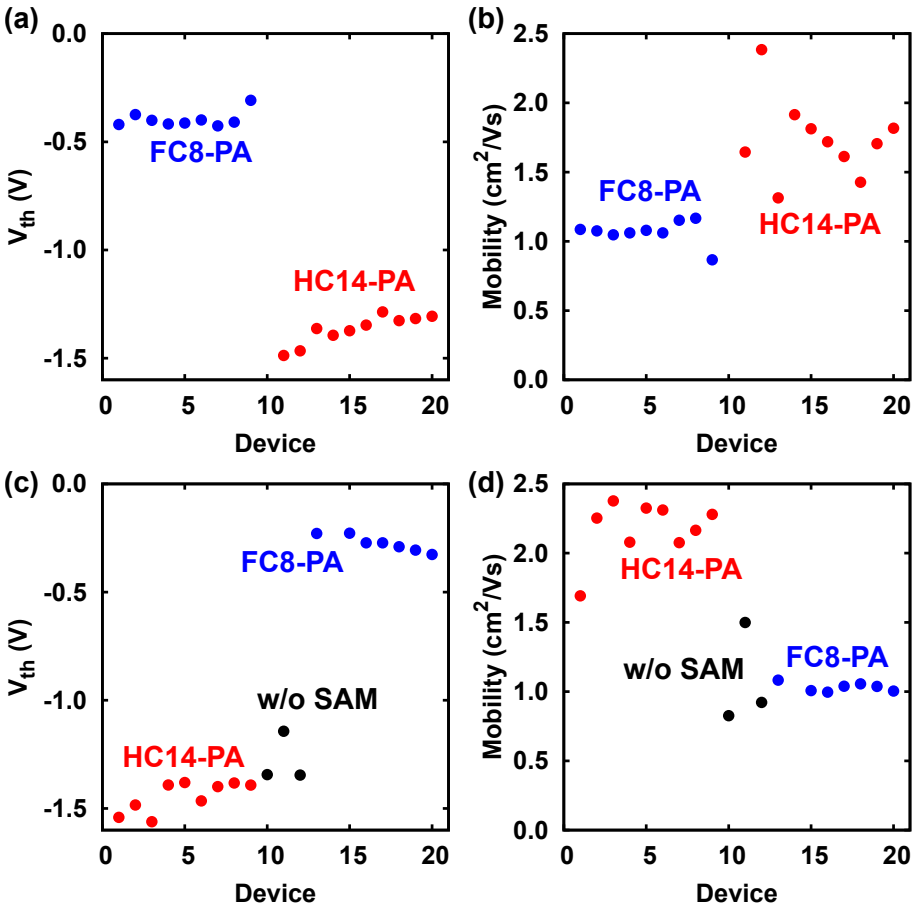

Figure 6.9: Threshold voltages and mobilities of transistors in sample 9S (without rinse) and 9T (with rinse). (a) Threshold voltages in sample 9S. (b) Threshold voltages in sample 9T. (c) Mobilities in sample 9S. (d) Mobilities in sample 9T. SAM in each transistor is colored according to the species.

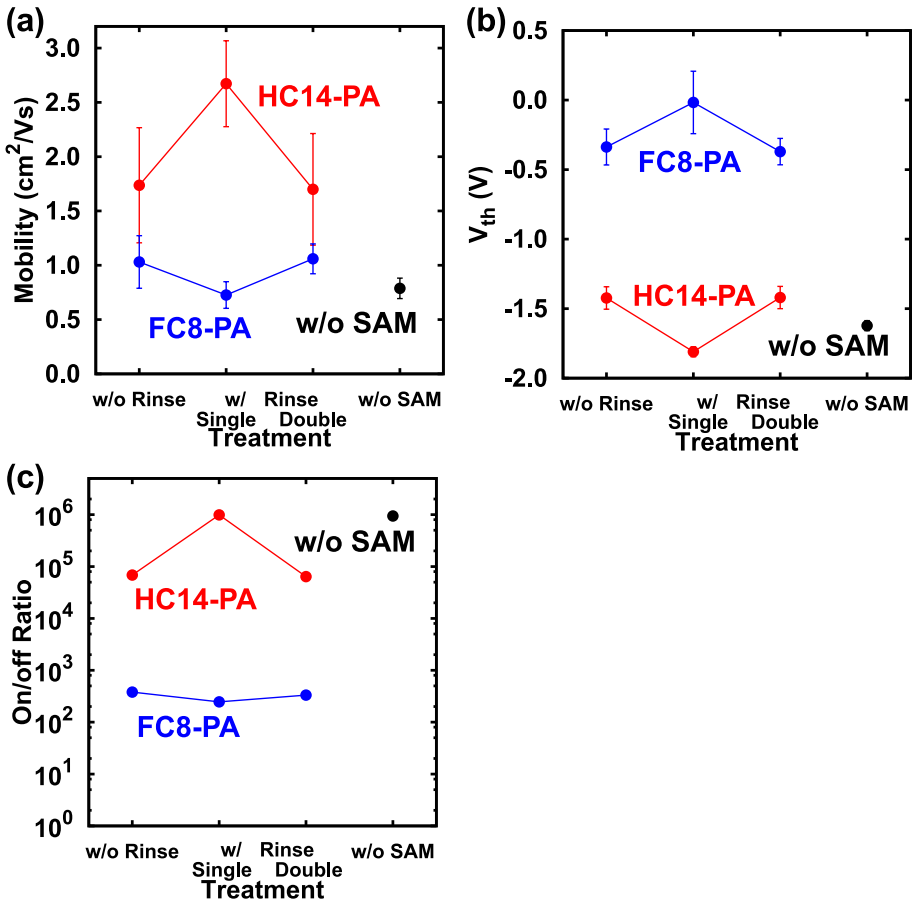

Figure 6.10: Summary of parameters of the samples in rinse effect investigation; (a) mobility, (b) threshed voltage, (c) on/off ratio. The plotted points are colored according to the SAM species. "Single" means that only single species of SAMs was rinsed at one time and "double" means that two species of SAMs were rinsed at one time.

Load Inverter

The input/output characteristics of the stamped load inverters are shown in Fig. 6.11 and those of dipped load inverters are shown in Fig. 6.12. In those figures, it can be seen that the threshold voltage of load inverter affects the switching voltage. When the load inverter was consisted of HC14-PA SAM, the switching voltage shifted to the negative direction. On the other hand, when the drive transistor was consisted of FC18-PA SAM, the switching voltage shifted to the positive direction. When the drive transistor consisted of HC14-PA SAM, the input/output characteristics always showed sharp drop around the switching voltage.

The switching voltage and gain extracted from the input/output characteristics are shown in Fig. 6.13.

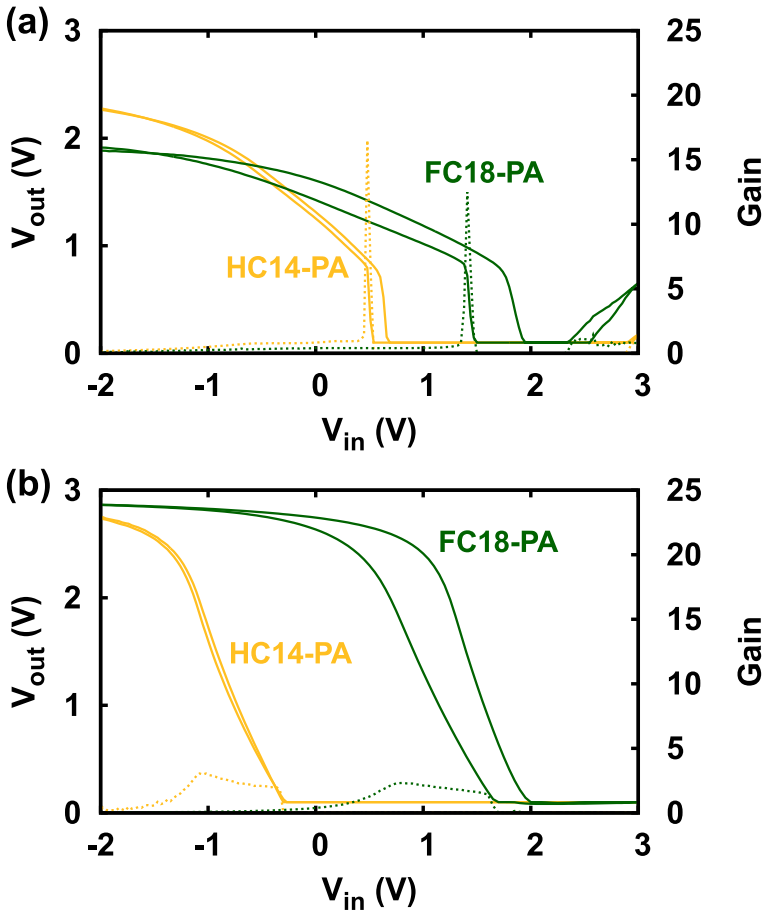

Figure 6.11: Input/output characteristics (solid line) and the gain (dotted line) of load inverters. All SAMs were formed by stamping. (a) Drive transistors have HC14-PA SAMs, while load inverters have HC14-PA SAMs (yellow) and FC18-PA SAMs (green), respectively. (b) Drive transistors have FC18-PA SAMs, while load inverters have HC14-PA SAMs (yellow) and FC18-PA SAMs (green), respectively.

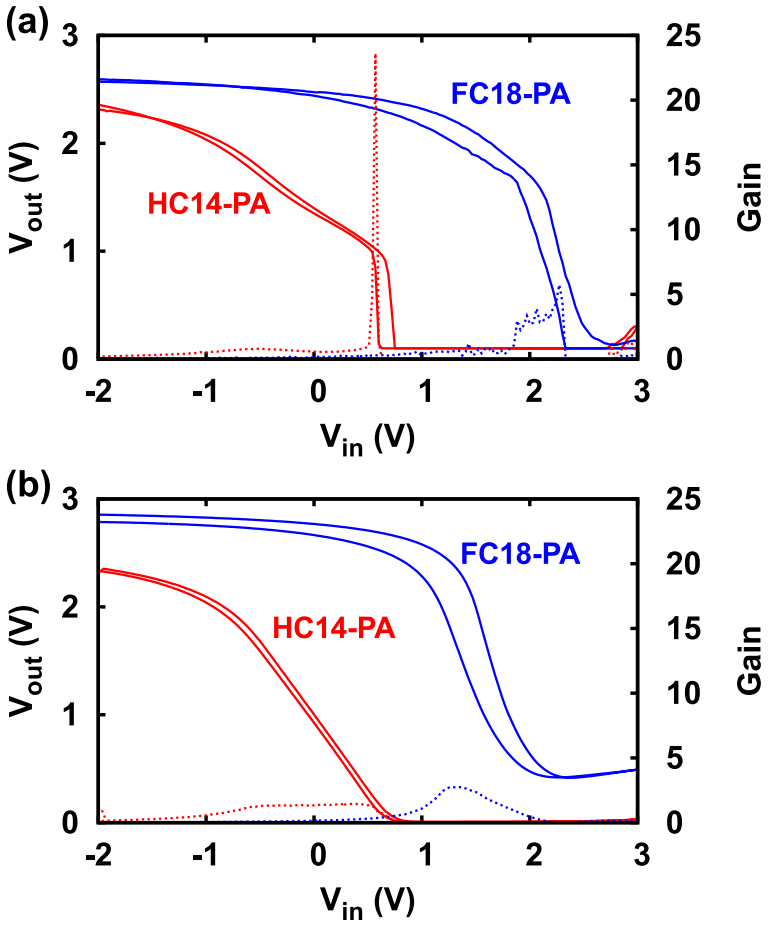

Figure 6.12: Input/output characteristics (solid line) and gain (dotted line) of load inverters. All SAMs were formed by dipping. (a) Drive transistors have HC14-PA SAMs, while load inverters have HC14-PA SAMs (yellow) and FC18-PA SAMs (green), respectively. (b) Drive transistors have FC18-PA SAMs, while load inverters have HC14-PA SAMs (yellow) and FC18-PA SAMs (green), respectively.

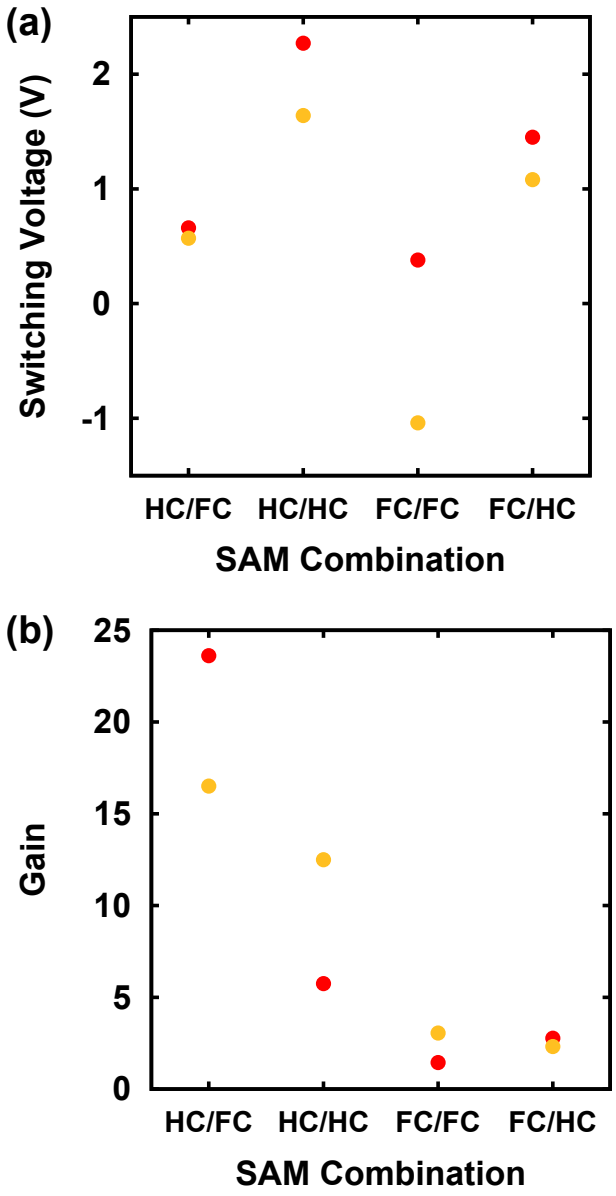

Figure 6.13: (a) Switching voltage and (b) gain of load inverters by stamping (yellow) and dipping (red). X-axis shows the species of SAMs in the load transistor M_{load} and the drive transistor M_{drive} as M_{load}/M_{load}.

6.3 Discussion

In this chapter, first the spatial formation of SAMs were performed. The equivalences of stamping process to dipping process was already proved in Chapter 5. Utilizing this stamping process, two species of SAMs were successfully transferred to a substrate simultaneously. The transistor characteristics were equivalent to those of the transistors by single-species stamping, and almost equivalent to those of dipped devices.

In the fabrication process, rinse has a role to remove the excess of SAM molecule and obtain uniform devices. Especially in the fabrication of large-sized devices, the uniformness is one of the critical keys. However, by stamping, there was a possibility that SAM molecules might contaminate. From the experiment, it was confirmed that the contamination by rinse did not occur by the threshold voltage and mobility in Fig. 6.9. Also, the difference in those values by rinse was not observed as shown in Fig. 5.5. The possibility of the contamination is considered by the coverage of the surface by stamping. When the substrate is rinsed, if the substrate has a region that is still activated and without SAM, the surface of the region cam be bond with the excess SAM molecule. However, from Chapter 5, it was confirmed that stamping of SAM formed dense monolayer without large SAM-free spaces. Therefore, by the nature of SAM molecules, only single monolayer was formed and excess molecules were removed by rinse without contamination.

Second, the spatial control of the threshold voltage by stamping was utilized in load inverter. The consistent of the switching voltage by SAM species was observed. By shifting the threshold voltage of load transistor to the positive direction, the switching voltage was also shifted to the positive direction, This phenomena can be ascribed to the conductance of the load transistor. When the load inverter consisted of FC8-PA-based transistor, due to the larger conductance in FC18-PA-based transistor, larger current flowed through the load and drive transistors. Therefore the voltage drop at the drive transistor became larger. The sharp drop in the load inverters with HC14-PA-based drive transistor is because of the smaller subthreshold swing of HC14-PA based transistors, as clearly shown in Fig. 6.5(a), (c) and Fig. 6.8(a), (c). Around $V_{\mathrm{GS}}= -1$ V, HC14-PA-based transistors had more decrease in the I_{DS}, therefore the sharp drop in output voltage and large gain were obtained.

Chapter 7

Conclusions and Future Work

7.1 Conclusions

In this work, structures and electric properties of SAMs transferred by microcontact printing (stamping) were closely observed and effects of parameters in the formation process were investigated.

- By contact angle measurement, the surface state of AlO_x was changed from hydrophobic to hydrophilic after stamping SAMs. Rinse had little effect to the surface state.
- By TEM observation of the cross-section of SAM capacitors, the existence of SAM on AlO_x was confirmed. The thickness of SAM layer was around 1 nm, which was consistent with the calculated value from the capacitance. In the cross-sectional picture, the SAM layer was smooth and no multilayer was observed.
- By NEXAFS measurement, the orientation, absorption intensity, and tilt angles of SAMs were measured. The NEXAFS PEY spectra of stamped SAMs were similar to the dipped SAMs and indicated that the spontaneous assemble of the molecules occurred on the stamped substrate, therefore stamping was proved to form self-assembled monolayers as like dipping. From absorption intensity and tilt angle of molecules, it was proved that the coverage was decreased by rinse then recovered by anneal.
- During the stamping, the effect of process parameters to the electric characteristics of SAMs and transistors were investigated. The concentration of the solution of SAMs had little effect to the formed SAMs. On the other hand, the stamping duration determined the transfer of SAM molecules. Critical duration was around 1 min, which was consistent with previous study of SAM formation by dipping [51]. As for the transistor characteristics, lower concentration, longer stamping duration, and annealing could achieve higher mobility and on/off ratio. Rinse decreased mobility, however, it also decreased parameter distribution.

- In large-size fabrication, the distribution of the stamped device became inevitably larger than that of the dipped device, though the distributions of stamped and dipped devices were equivalent in small-size fabrication. However, the order of distribution in dipped sample and stamped sample was always equivalent.

Furthermore, a new method to control the threshold voltage of organic TFTs utilizing the stamping process was proposed and experimented. The critical problem in this method was the rinse, whether the SAMs are contaminated or not by rinse. In the experiments, the contamination was not observed and the effect of rinse to transistor characteristics was proved to be almost negligible.

- Formation of more than one species of SAM on a substrate was demonstrated by utilizing stamping. According to the geometry, the difference of the threshold voltage and mobility was clearly observed.

- Rinse was proved not to cause contamination, when a substrate with more than one species of SAM was rinsed. The difference in the transistor characteristics between rinsed sample with single species of SAM and rinsed sample with two species of SAMs was negligibly small.

- Load inverters consisting of transistors with different threshold voltages were fabricated and input/output characteristics were measured. The largest difference in the switching voltage was 1.89 V under the driving voltage of -3 V.

Through this work, stamping of SAMs is analyzed and established, then utilized in the spatial control of the threshold voltage in organic transistors. Spatial control of the threshold voltage using solution process was not reported before. Stamping fulfills the requirements for the threshold voltage control; controllability, preciseness, stability, low-operation voltage, reproducibility, and process simpleness. By stamping to enable spatial control of the devices, the possibility of organic transistors and circuits would be expanded largely.

7.2 Future Work

Stamping can be applied for more complicated circuits that require precise and deterministic control of device characteristics. In addition to the ability to control the threshold voltage, stamping has other advantages. One of them is that in stamping process, very little volume of solution is required though stamping is classified as a solution process, therefore this method enables the fabrication of organic transistors on fusible substrates.

One of the characteristics of organic transistors is low process temperature. Because of the low temperature, fabrication of the transistors on unconventional substrates such as plastic films and paper [54] is enabled beside conventional silicon and glass substrates. Making the most of this characteristics, nowadays the application of organic electronics to medical use such as *in vivo* biosensors is prospected.

For *in vivo* measurement, there are many requirements such as sensitivity and low voltage operation. As for the sensitivity, the best method is to fabricate the sensors on the living body, or otherwise on biocompatible substrates that fuse in living body. However, those substrates are often fusible to the solvents. As for the low voltage operation, the combination of AlO_x and phosphonic acid SAM gate dielectrics is regarded to be appropriate. However, in the conventional method, the formation of phosphonic acid SAM requires the solution of SAM, which can do damage to the substrate. On the other hand, stamping requires very small volume of the solution, therefore the damage to the substrate can be minimized.

Above is one of the examples, though, there is a vast space to fully exploit the advantages and characteristics of organic electronics. The author strongly hopes that the stamping method contributes to the future development of organic electronics.

List of publication

Journal Papers

1. I. Hirata, U. Zschieschang, F. Ante, T. Yokota, K. Kuribara, T. Yamamoto, K. Takimiya, M. Ikeda, H. Kuwabara, H. Klauk, T. Sekitani, and T. Someya, "Spatial control of the threshold voltage of low-voltage organic transistors by microcontact printing of alkyl- and fluoroalkyl-phosphonic acids," *MRS Communications*, vol. 1, no. 1, pp. 1–4, Aug. 2011.

International Conferences (refereed)

1. I. Hirata, U. Zschieschang, F. Ante, T. Yokota, K. Kuribara, T. Yamamoto, K. Takimiya, M. Ikeda, H. Kuwabara, H. Klauk, T. Sekitani, and T. Someya, "Spatial Control of the Threshold Voltage of Low-Voltage Organic Transistors by Microcontact Printing of Alkyl- and Fluoroalkyl-phosphonic Acids," in *2*011 International Conference on Solid State Devices and Materials (SSDM 2011), 2011, B-3-4.

2. I. Hirata, U. Zschieschang, F. Ante, T. Yokota, K. Kuribara, T. Yamamoto, K. Takimiya, M. Ikeda, H. Kuwabara, H. Klauk, T. Sekitani, and T. Someya, "Stamping of a Self-assembled Monolayer for Organic Circuits with Spatially Controlled Threshold Voltages" in *2*012 MRS Spring Meeting, 2012 (accepted).

Domestic Conferences (non-refereed)

1. 平田郁恵, Ute Zschieschang, Frederik Ante, Hagen Klauk, 関谷 毅, 山本 達也, 瀧宮 和男, 池田 征明, 桑原 博一, 染谷 隆夫, 「スタンプ法による低電圧駆動有機トランジスタの閾値電圧制御」, 2011 年春季 第 58 回 応用物理学会関係連合講演会, 2011 年 3 月.

2. 平田 郁恵, Ute Zschieschang, Frederik Ante, 横田 知之, 栗原 一徳, 山本 達也, 瀧宮 和男, 池田 征明, 桑原 博一, Hagen Klauk, 関谷 毅, 染谷 隆夫, 「スタンプ法による低電圧駆動有機インバータのスイッチ電圧制御」, 2011 年秋季 第 72 回 応用物理学会学術講演会, 2011 年 8 月, 31a-R-10.

3. 平田 郁恵, Ute Zschieschang, Frederik Ante, 横田 知之, 栗原 一徳, 山本 達也, 瀧宮 和男, 池田 征明, 桑原 博一, Hagen Klauk, 関谷 毅, 染谷 隆夫, 「スタンプ法による自己組織化単分子膜の観察と高解像度局所制御」, 2012 年春季 第 59 回 応用物理学会関係連合講演会, 2012 年 3 月, 15p-GP11-21 (予定).

Acknowledgment

This work could not be completed without the help from those who supported me through my master course. First, I would like to thank my advisers, Professor Takao Someya and Associate Professor Tsuyoshi Sekitani, for their help, advice, and discussions. Among their guidance, what I thank them the most is that they introduced me into the fascinating field of organic electronics. The organic electronics world, including devices from the basics to the application, and even the situation that organic electronics is in the early state of development, was very novel and exciting to me, a researcher in inorganic electronics. My gratitude lies in the path, on which I have chosen this field and found my place in their group. Also, for their kindness, my two-month stay in Max-Planck Institute gave me a lot of insights not only to my master course topic but also to my decision to pursue the research further.

I would like to acknowledge our many collaborators: Dr. Hagen Klauk, Dr. Ute Zschieschang, Dr. Frederik Ante, Daniel Kaelblein, Hyeyeon Ryu, Ulrike Kraft, Thomas Egerer in Max-Planck Institute. This work was proposed during my stay in Max-Planck Institute. With their kind help and education, I was able to chose this topic for my thesis.

I would like to show my gratitude to Professor Yueh-Lin Loo and He Wang in Princeton University, for their help in NEXAFS measurement. With their support in NEXAFS measurement, the critical question in SAM formation was revealed.

I owe my thanks to members (former and current) of Someya and Sekitani group: Dr. Kenjiro Fukuda, Tomoyuki Yokota, Kazunori Kuribara, Takashi Nakagawa, who always trained me in the machine operation, experimental processes, and scientific writing and gave me a lot of practical advice as senior students in the group; Yu Kato, for always being a good and keen colleague and having driven my eagerness; Takeyoshi Tokuhara, Jun Miura, for their serious attitude toward research that taught me a lot; Naoya Take, Tatsuya Terakawa, Naoji Matsuhisa, and Shigeyoshi Ito, for their earnestness in studying and learning for their own projects.

I would like to acknowledge foreign researchers and students: Dr. Zhao Yiying, Sung Won Lee, Dr. Soorathep Kheawhom, and especially Martin Kaltenbrunner, for his inspiring study and always fruitful discussions.

I would like to thank the secretaries in Someya and Sekitani group, Remi Takano, Kazuyo Matsuoka, Youko Tashiro, Shoko Yamazaki, and Fumie Imabayashi for business transactions, for their continuous hard work to keep the office and laboratory enjoyable,

and for occasional chat in the afternoon.

I also would like to show my gratitude to my friends in the faculty. Many discussions on many subjects, including our major to sometimes beyond academic topics, always gave me inspiration, encouragement, and prefaces to ponder over significance of our times.

Last but not least, nothing can express my full gratitude to my family, far but caring about me carrying through my work.

Bibliography

[1] J. Bardeen and W. Brattain, "The Transistor, A Semi-Conductor Triode," *Physical Review*, vol. 74, no. 2, pp. 230–231, Jul. 1948.

[2] J. Bokor, E. Anderson, C. Kuo, K. Asano, H. Takeuchi, J. Kedzierski, and D. Hisamoto, "FinFET-a self-aligned double-gate MOSFET scalable to 20 nm," *IEEE Transactions on Electron Devices*, vol. 47, no. 12, pp. 2320–2325, 2000.

[3] H. Klauk, U. Zschieschang, J. Pflaum, and M. Halik, "Ultralow-power organic complementary circuits." *Nature*, vol. 445, no. 7129, pp. 745–8, Feb. 2007.

[4] J. A. Rogers, Z. Bao, K. Baldwin, A. Dodabalapur, B. Crone, V. R. Raju, V. Kuck, H. E. H. Katz, K. Amundson, J. Ewing, and P. Drzaic, "Paper-like electronic displays: large-area rubber-stamped plastic sheets of electronics and microencapsulated electrophoretic inks." *Proceedings of the National Academy of Sciences of the United States of America*, vol. 98, no. 9, pp. 4835–40, Apr. 2001.

[5] A. Dodabalapur, Z. Bao, A. Makhija, J. G. Laquindanum, V. R. Raju, Y. Feng, H. E. H. Katz, and J. A. Rogers, "Organic smart pixels," *Applied Physics Letters*, vol. 73, no. 2, p. 142, 1998.

[6] K. Myny, S. Steudel, S. Smout, P. Vicca, F. Furthner, B. Van Der Putten, A. Tripathi, G. Gelinck, J. Genoe, W. Dehaene, and P. Heremans, "Organic RFID transponder chip with data rate compatible with electronic product coding," *Organic Electronics*, vol. 11, no. 7, pp. 1176–1179, 2010.

[7] K. Myny, E. van Veenendaal, G. H. Gelinck, J. Genoe, W. Dehaene, and P. Heremans, "An 8b organic microprocessor on plastic foil," in *2011 IEEE International Solid-State Circuits Conference*. IEEE, Feb. 2011, pp. 322–324.

[8] B. J. Jung, K. Lee, J. Sun, A. G. Andreou, and H. E. Katz, "Air-Operable, High-Mobility Organic Transistors with Semifluorinated Side Chains and Unsubstituted Naphthalenetetracarboxylic Diimide Cores: High Mobility and Environmental and Bias Stress Stability from the Perfluorooctylpropyl Side Chain," *Advanced Functional Materials*, pp. n/a–n/a, Jul. 2010.

[9] T. Someya, T. Sekitani, S. Iba, Y. Kato, H. Kawaguchi, and T. Sakurai, "A large-area, flexible pressure sensor matrix with organic field-effect transistors for

artificial skin applications." *Proceedings of the National Academy of Sciences of the United States of America*, vol. 101, no. 27, pp. 9966–70, Jul. 2004.

[10] T. Someya, Y. Kato, T. Sekitani, S. Iba, Y. Noguchi, Y. Murase, H. Kawaguchi, and T. Sakurai, "Conformable, flexible, large-area networks of pressure and thermal sensors with organic transistor active matrixes." *Proceedings of the National Academy of Sciences of the United States of America*, vol. 102, no. 35, pp. 12 321–5, Aug. 2005.

[11] T. Someya, Y. Kato, S. Iba, Y. Noguchi, T. Sekitani, H. Kawaguchi, and T. Sakurai, "Integration of Organic FETs With Organic Photodiodes for a Large Area, Flexible, and Lightweight Sheet Image Scanners," *IEEE Transactions on Electron Devices*, vol. 52, no. 11, pp. 2502–2511, Nov. 2005.

[12] M. Takamiya, T. Sekitani, Y. Kato, H. Kawaguchi, T. Someya, and T. Sakurai, "An Organic FET SRAM for Braille Sheet Display with Back Gate to Increase Static Noise Margin," in *2006 IEEE International Solid State Circuits Conference - Digest of Technical Papers*. IEEE, 2006, pp. 1060–1069.

[13] T. Sekitani, Y. Noguchi, K. Hata, T. Fukushima, T. Aida, and T. Someya, "A rubberlike stretchable active matrix using elastic conductors," *Science*, vol. 321, no. 5895, p. 1468, Sep. 2008.

[14] T. Sekitani, T. Yokota, U. Zschieschang, H. Klauk, S. Bauer, K. Takeuchi, M. Takamiya, T. Sakurai, and T. Someya, "Organic nonvolatile memory transistors for flexible sensor arrays," *Science*, vol. 326, no. 5959, pp. 1516–9, Dec. 2009.

[15] T. Sekitani, H. Nakajima, H. Maeda, T. Fukushima, T. Aida, K. Hata, and T. Someya, "Stretchable active-matrix organic light-emitting diode display using printable elastic conductors." *Nature Materials*, vol. 8, no. 6, pp. 494–9, Jun. 2009.

[16] E. Cantatore and E. Meijer, "Transistor operation and circuit performance in organic electronics," in *ESSCIRC 2004 - 29th European Solid-State Circuits Conference*. IEEE, 2004, pp. 29–36.

[17] U. Kraft, U. Zschieschang, F. Ante, D. Kälblein, C. Kamella, K. Amsharov, M. Jansen, K. Kern, E. Weber, and H. Klauk, "Fluoroalkylphosphonic acid self-assembled monolayer gate dielectrics for threshold-voltage control in low-voltage organic thin-film transistors," *Journal of Materials Chemistry*, vol. 20, no. 31, p. 6416, 2010.

[18] U. Zschieschang, F. Ante, M. Schlörholz, M. Schmidt, K. Kern, and H. Klauk, "Mixed self-assembled monolayer gate dielectrics for continuous threshold voltage control in organic transistors and circuits." *Advanced Materials*, vol. 22, no. 40, pp. 4489–93, Oct. 2010.

[19] U. Zschieschang, M. Halik, and H. Klauk, "Microcontact-printed self-assembled monolayers as ultrathin gate dielectrics in organic thin-film transistors and complementary circuits." *Langmuir*, vol. 24, no. 5, pp. 1665–9, Mar. 2008.

[20] 薄膜材料デバイス研究会, **薄膜トランジスタ**, 2nd ed., 薄膜材料デバイス研究会, Ed. コロナ社.

[21] K. Fukuda, T. Hamamoto, T. Yokota, T. Sekitani, U. Zschieschang, H. Klauk, and T. Someya, "Effects of the alkyl chain length in phosphonic acid self-assembled monolayer gate dielectrics on the performance and stability of low-voltage organic thin-film transistors," *Applied Physics Letters*, vol. 95, no. 20, p. 203301, 2009.

[22] D. Gundlach, Y. Lin, T. Jackson, S. Nelson, and D. Schlom, "Pentacene organic thin-film transistors-molecular ordering and mobility," *IEEE Electron Device Letters*, vol. 18, no. 3, pp. 87–89, Mar. 1997.

[23] D. J. Gundlach, J. A. Nichols, L. Zhou, and T. N. Jackson, "Thin-film transistors based on well-ordered thermally evaporated naphthacene films," *Applied Physics Letters*, vol. 80, no. 16, p. 2925, 2002.

[24] K. Takimiya, T. Yamamoto, H. Ebata, and T. Izawa, "Design strategy for air-stable organic semiconductors applicable to high-performance field-effect transistors," *Science and Technology of Advanced Materials*, vol. 8, no. 4, pp. 273–276, May 2007.

[25] Y.-L. Loo, R. L. Willett, K. W. Baldwin, and J. A. Rogers, "Interfacial Chemistries for Nanoscale Transfer Printing," *Journal of the American Chemical Society*, vol. 124, no. 26, pp. 7654–7655, Jul. 2002.

[26] R. Luschtinetz, A. F. Oliveira, H. A. Duarte, and G. Seifert, "Self-assembled Monolayers of Alkylphosphonic Acids on Aluminum Oxide Surfaces - A Theoretical Study," *Zeitschrift für anorganische und allgemeine Chemie*, vol. 636, no. 8, pp. 1506–1512, May 2010.

[27] H. Klauk, U. Zschieschang, and M. Halik, "Low-voltage organic thin-film transistors with large transconductance," *Journal of Applied Physics*, vol. 102, no. 7, p. 074514, 2007.

[28] Y. Abe, T. Hasegawa, Y. Takahashi, T. Yamada, and Y. Tokura, "Control of threshold voltage in pentacene thin-film transistors using carrier doping at the charge-transfer interface with organic acceptors," *Applied Physics Letters*, vol. 87, no. 15, p. 153506, 2005.

[29] H. Kawaguchi, M. Taniguchi, and T. Kawai, "Control of threshold voltage and hysteresis in organic field-effect transistors," *Applied Physics Letters*, vol. 94, no. 9, p. 093305, 2009.

[30] J. Koo, J. Lim, S. Kim, S. Yun, C. Ku, S. Lim, and J. Lee, "Pentacene thin-film transistors and inverters with plasma-enhanced atomic-layer-deposited Al2O3 gate dielectric," *Thin Solid Films*, vol. 515, no. 5, pp. 3132–3137, Jan. 2007.

[31] S. Kobayashi, T. Nishikawa, T. Takenobu, S. Mori, T. Shimoda, T. Mitani, H. Shimotani, N. Yoshimoto, S. Ogawa, and Y. Iwasa, "Control of carrier density by self-assembled monolayers in organic field-effect transistors." *Nature materials*, vol. 3, no. 5, pp. 317–22, May 2004.

[32] K. P. Pernstich, S. Haas, D. Oberhoff, C. Goldmann, D. J. Gundlach, B. Batlogg, a. N. Rashid, and G. Schitter, "Threshold voltage shift in organic field effect transistors by dipole monolayers on the gate insulator," *Journal of Applied Physics*, vol. 96, no. 11, p. 6431, 2004.

[33] U. Zschieschang, F. Ante, M. Schlorholz, K. Kern, and H. Klauk, *Deterministic and continuous control of the threshold voltage and noise margin of organic thin-film transistors and organic complementary circuits using mixed phosphonic acid self-assembled monolayer gate dielectrics.* IEEE, Jun. 2009.

[34] S. Iba, T. Sekitani, Y. Kato, T. Someya, H. Kawaguchi, M. Takamiya, T. Sakurai, and S. Takagi, "Control of threshold voltage of organic field-effect transistors with double-gate structures," *Applied Physics Letters*, vol. 87, no. 2, p. 023509, 2005.

[35] K. Hizu, T. Sekitani, T. Someya, and J. Otsuki, "Reduction in operation voltage of complementary organic thin-film transistor inverter circuits using double-gate structures," *Applied Physics Letters*, vol. 90, no. 9, p. 093504, 2007.

[36] T. Yokota, T. Nakagawa, T. Sekitani, Y. Noguchi, K. Fukuda, U. Zschieschang, H. Klauk, K. Takeuchi, M. Takamiya, T. Sakurai, and T. Someya, "Control of threshold voltage in low-voltage organic complementary inverter circuits with floating gate structures," *Applied Physics Letters*, vol. 98, no. 19, p. 193302, 2011.

[37] D. Qin, Y. Xia, and G. M. Whitesides, "Soft lithography for micro- and nanoscale patterning." *Nature protocols*, vol. 5, no. 3, pp. 491–502, Jan. 2010.

[38] A. Kumar and G. M. Whitesides, "Features of gold having micrometer to centimeter dimensions can be formed through a combination of stamping with an elastomeric stamp and an alkanethiol ‘‘ ink ’’ followed by chemical etching," *Applied Physics Letters*, vol. 63, no. 14, p. 2002, 1993.

[39] M. Mrksich and G. M. Whitesides, "Patterning self-assembled monolayers using microcontact printing: A new technology for biosensors?" *Trends in Biotechnology*, vol. 13, no. 6, pp. 228–235, Jun. 1995.

[40] J. Zaumseil, M. A. Meitl, J. W. P. Hsu, B. R. Acharya, K. W. Baldwin, Y.-L. Loo, and J. A. Rogers, "Three-Dimensional and Multilayer Nanostructures Formed by Nanotransfer Printing," *Nano Letters*, vol. 3, no. 9, pp. 1223–1227, Sep. 2003.

[41] M. M. Stevens, M. Mayer, D. G. Anderson, D. B. Weibel, G. M. Whitesides, and R. Langer, "Direct patterning of mammalian cells onto porous tissue engineering substrates using agarose stamps." *Biomaterials*, vol. 26, no. 36, pp. 7636–41, Dec. 2005.

[42] Y.-L. Loo, R. L. Willett, K. W. Baldwin, and J. A. Rogers, "Additive, nanoscale patterning of metal films with a stamp and a surface chemistry mediated transfer process: Applications in plastic electronics," *Applied Physics Letters*, vol. 81, no. 3, p. 562, 2002.

[43] T. Young, "An Essay on the Cohesion of Fluids," *Philosophical Transactions of the Royal Society of London*, vol. 95, pp. 65–87, Jan. 1805.

[44] D. Kwok and A. Neumann, "Contact angle measurement and contact angle interpretation," *Advances in Colloid and Interface Science*, vol. 81, no. 3, pp. 167–249, Sep. 1999.

[45] M.-W. Yang and S.-Y. Lin, "A method for correcting the contact angle from the $\theta/2$ method," *Colloids and Surfaces A: Physicochemical and Engineering Aspects*, vol. 220, no. 1-3, pp. 199–210, Jun. 2003.

[46] J. Stöhr, *NEXAFS spectroscopy*. Springer, 1992.

[47] B. Watts, L. Thomsen, and P. Dastoor, "Methods in carbon K-edge NEXAFS: Experiment and analysis," *Journal of Electron Spectroscopy and Related Phenomena*, vol. 151, no. 2, pp. 105–120, Apr. 2006.

[48] M. G. Samant, J. Stöhr, H. R. Brown, T. P. Russell, J. M. Sands, and S. K. Kumar, "NEXAFS Studies on the Surface Orientation of Buffed Polyimides," *Macromolecules*, vol. 29, no. 26, pp. 8334–8342, Jan. 1996.

[49] P. Fontaine, D. Goguenheim, D. Deresmes, D. Vuillaume, M. Garet, and F. Rondelez, "Octadecyltrichlorosilane monolayers as ultrathin gate insulating films in metal-insulator-semiconductor devices," *Applied Physics Letters*, vol. 62, no. 18, pp. 2256–2258, 1993.

[50] A. Jedaa, M. Burkhardt, U. Zschieschang, H. Klauk, D. Habich, G. Schmid, and M. Halik, "The impact of self-assembled monolayer thickness in hybrid gate dielectrics for organic thin-film transistors," *Organic Electronics*, vol. 10, no. 8, pp. 1442–1447, Dec. 2009.

[51] C. Bram, C. Jung, and M. Stratmann, "Self assembled molecular monolayers on oxidized inhomogeneous aluminum surfaces," *Fresenius' Journal of Analytical Chemistry*, vol. 358, no. 1-2, pp. 108–111, May 1997.

[52] J. T. Woodward and D. K. Schwartz, "In Situ Observation of Self-Assembled Monolayer Growth," *Journal of the American Chemical Society*, vol. 118, no. 33, pp. 7861–7862, Jan. 1996.

[53] R. Maoz and J. Sagiv, "On the formation and structure of self-assembling monolayers. I. A comparative atr-wettability study of Langmuir—Blodgett and adsorbed films on flat substrates and glass microbeads," *Journal of Colloid and Interface Science*, vol. 100, no. 2, pp. 465–496, Aug. 1984.

[54] F. Eder, H. Klauk, M. Halik, U. Zschieschang, G. Schmid, and C. Dehm, "Organic electronics on paper," *Applied Physics Letters*, vol. 84, no. 14, p. 2673, 2004.